

## Target-Mediated Drug Disposition Affects the Pharmacokinetics of Interleukin-10 Fc-fusion Proteins at Pharmacologically Active Doses

**Authors:** Zheng Yang, Surendran Rajendran, Vanessa Spires, Brian Poirson, Murali Gururajan, Zheng Lin, Jaren Arbanas, Stanley Krystek, James Loy, Yuan Cheng, Stephen Carl, Samantha Pace, Yun Wang, John Mehl, Shihua Xu, Krishna Vasudevan, Miranda Broz, Lois Lehman-McKeeman, Paul Morin, and Robert F. Graziano

**Affiliation:** Metabolism and Pharmacokinetics, Pharmaceutical Candidate Optimization, Bristol Myers Squibb Company, Princeton, New Jersey, U.S.A. (Z.Y.); Nonclinical Disposition and Bioanalysis, Bristol Myers Squibb Company, Princeton, New Jersey, U.S.A. (S.R., S.X.); Discovery Biotherapeutics, Bristol Myers Squibb Company, Princeton, New Jersey, U.S.A. (Z.L., J.A., P.M.); Molecular Structure and Design, Bristol Myers Squibb Company, Princeton, New Jersey, U.S.A. (S.K.); Discovery Toxicology, Pharmaceutical Candidate Optimization, Bristol Myers Squibb Company, Cambridge, Massachusetts, U.S.A. (J.L.); Discovery Pharmaceuticals and Analytical Sciences, Pharmaceutical Candidate Optimization, Bristol Myers Squibb Company, Princeton, New Jersey, U.S.A. (Y.C., S.C., S.P., Y.W., J.M.); Discovery Oncology, Bristol Myers Squibb Company, Princeton, New Jersey, U.S.A. (V.S., B.P., M.G., R.F.G.); Translational Medicine, Bristol Myers Squibb Company, Princeton, New Jersey, U.S.A. (K.V.); Discovery Oncology, Bristol Myers Squibb Company, Redwood City, California, U.S.A. (M.B.); Pharmaceutical Candidate Optimization, Bristol Myers Squibb Company, Princeton, New Jersey, U.S.A. (L.L-M.)

**Running Title:** TMDD Affects PK of IL-10 Fc-fusion Proteins

**Corresponding Author:** Zheng Yang, Route 206 and Province Line Road, Bristol Myers

Squibb Company, Princeton, NJ 08543-4000. Telephone: (609) 252-4595; Facsimile: (609) 252-7354; E-mail: [yangz@bms.com](mailto:yangz@bms.com)

**Number of Text Pages:** 42

**Number of Tables:** 6

**Number of Figures:** 6

**Number of Words in Abstract:** 250

**Number of Words in Introduction:** 624

**Number of Words in Discussion:** 1455

**Abbreviations:**  $A_{IP}$ , amount of drug at the intraperitoneal absorption site;  $A_{peripheral}$ , amount of drug in the peripheral compartment;  $AUC_{tot}$ , area under the drug concentration-time curve;  $C_{max}$ , peak concentration;  $C_p$ , drug plasma or serum concentration in the central compartment;  $CL_{tot}$ , total body clearance; Fc, fragment crystallizable; hFc, human fragment crystallizable; hIL-10, human interleukin-10; IL-10, interleukin-10; IP, intraperitoneal; IV, intravenous;  $k_{12}$ , transfer rate constant from the central to the peripheral compartment;  $k_{21}$ , transfer rate constant from the peripheral to the central compartment;  $k_a$ , absorption rate constant  $k_{el,non-target-mediated}$ , non-target-mediated first-order elimination rate constant;  $K_m$ , binding affinity to target; mAb, monoclonal antibody; mFc, mouse fragment crystallizable; mIL-10, mouse interleukin-10; mPD-1, mouse programmed death-1; PD-1, programmed death-1;  $t_{1/2}$ , terminal half-life;  $V_c$ , volume of

distribution in the central compartment;  $V_{c, \text{apparent}}$ , apparent volume of distribution in the central compartment after intraperitoneal administration;  $V_{\text{max}, \text{target-mediated}}$ , maximum elimination rate mediated by target;  $V_{ss}$ , steady-state volume of distribution

## ABSTRACT

Fragment crystallizable (Fc) fusion is commonly used for extending the half-life of biotherapeutics such as cytokines. In this work, we studied the pharmacokinetics of Fc-fused interleukin-10 (IL-10) proteins that exhibited potent antitumor activity in mouse syngeneic tumor models. At pharmacologically active doses of  $\geq 0.1$  mg/kg, both mouse Fc-mouse IL-10 and human Fc-human IL-10, constructed as the C-terminus of the Fc domain fused with IL-10 via a glycine-serine polypeptide linker, exhibited nonlinear pharmacokinetics after intravenous administration to mice at the doses of 0.05, 0.5, and 5 mg/kg. With a nominal dose ratio of 1:10:100; the ratio of the area under the curve for mouse Fc-mouse IL-10 and human Fc-human IL-10 was 1:181:1830 and 1:75:633, respectively. In contrast, recombinant mouse or human IL-10 proteins exhibited linear pharmacokinetics in mice. Compartmental analysis, using the Michaelis-Menten equation with the in vitro IL-10 receptor alpha binding affinity inputted as the  $K_m$ , unified the pharmacokinetic data across the dose range. Additionally, non-target-mediated clearance estimated for fusion proteins was  $\sim 200$ -fold slower than that for cytokines, causing the manifestation of target-mediated drug disposition (TMDD) in the fusion protein pharmacokinetics. The experimental data generated with a mouse IL-10 receptor alpha-blocking antibody and a human Fc-human IL-10 mutant with a reduced receptor binding affinity showed significant improvements in pharmacokinetics, supporting TMDD as the cause of nonlinearity. Target expression and its effect on pharmacokinetics must be determined when considering using Fc as a half-life extension strategy, and pharmacokinetic evaluations need to be performed at a range of doses covering pharmacological activity.

## **SIGNIFICANCE STATEMENT**

Target-mediated drug disposition can manifest to affect the pharmacokinetics of a fragment crystallizable (Fc)-fused cytokine when the non-target-mediated clearance of the cytokine is decreased due to neonatal Fc receptor-mediated recycling and molecular weight increases that reduce the renal clearance. The phenomenon was demonstrated with interleukin-10 Fc-fusion proteins in mice at pharmacologically active doses. Future drug designs using Fc as a half-life extension approach for cytokines need to consider target expression and its effect on pharmacokinetics at relevant doses.

## INTRODUCTION

Interleukin-10 (IL-10) belongs to the IL-10-interferon cytokine family and is a multifunctional dimeric cytokine produced by many immune cells such as T cells, B cells, and natural killer cells (Moore et al., 2001; Shouval et al., 2014). IL-10 binds to the IL-10 receptor alpha with a high affinity (0.035-0.24 nM) (Moore et al., 2001; Walter, 2014). Upon the binding, it leads to the recruitment of the IL-10 receptor beta and produces a complex signaling cascade, including the phosphorylation of signal transducer and activator of transcription 3 (STAT3). The IL-10 receptor alpha is expressed by hematopoietic cells. Although the expression of the IL-10 receptor alpha was reported to be a few hundred per cell (Moore et al., 2001, von Haehling et al., 2015), a wide expression of the receptor in many immune cells renders meaningful target concentrations in blood and tissues such as the spleen, thymus, and lymph node (Liu et al., 1994), which leads to the diverse effects of IL-10 that are both anti-inflammatory and immunostimulatory. Because of the pro-inflammatory effect of IL-10, it was explored as an immuno-oncologic agent for treating cancer. Preclinically, the IL-10 treatment in mice led to the expansion and activation of primed CD8<sup>+</sup> T cells and NK cells, which resulted in the regression of mouse syngeneic tumors (Berman et al., 1996; Adris et al., 1999; Mumm et al., 2011; Emmerich et al., 2012). Clinically, pegilodecakin, a PEGylated IL-10, induced CD8<sup>+</sup> T cell-mediated immunity in cancer patients (Naing et al., 2018). While pegylated IL-10 did not improve efficacy in the Phase III trial of advanced pancreatic cancer (Hecht et al., 2021), it showed an improvement in the overall response rate (44% versus the historical data of 20%) when combined with anti-programmed death-1 (PD-1) antibodies in the heavily pretreated renal cell carcinoma patient population, warranting the further investigation of the IL-10 treatment (Tannir, et al., 2021).

Fragment crystallizable (Fc) fusion is a commonly employed method to extend the half-life ( $t_{1/2}$ ) of peptides, antibody fragments, cytokines, and receptor extracellular domains (Kontermann., 2016). The mechanisms of the  $t_{1/2}$  extension are presumably due to the molecular weight increases that reduce the size-dependent renal filtration and the neonatal Fc receptor (FcRn)-mediated recycling. Cytokines exhibit short  $t_{1/2}$  of a few hours in humans, resulting in the requirement for more frequent dosing regimens in the clinic. For example, recombinant interferon alpha-2b (Intron<sup>®</sup>-A) has a  $t_{1/2}$  of 2-3 hours (Intron<sup>®</sup>-A package insert), and the  $t_{1/2}$  of recombinant interferon alpha-2a (Roferon<sup>®</sup>-A) ranges from 3.7 to 8.5 hours (Roferon<sup>®</sup>-A package insert). Similarly, recombinant IL-2 (aldesleukin, Proleukin<sup>®</sup>) exhibits a terminal  $t_{1/2}$  of 1.4 hours in humans (Proleukin<sup>®</sup> package insert). Given the therapeutic potential of cytokines (Runbeck et al., 2021) and their short circulating  $t_{1/2}$  in general, they may be suitable candidates for Fc fusion. In the literature, Fc-fusion proteins with IL-2, IL-12, and IL-15 were reported for the  $t_{1/2}$  extension and antitumor activities (Zhu et al., 2015; Rhode et al., 2016; Vazquez-Lombardi et al., 2017; Jung et al., 2018).

The objectives of the research were to evaluate the pharmacokinetics (PK) of IL-10 Fc-fusion proteins (Figure 1) and investigate the cause of nonlinear PK and a short  $t_{1/2}$  (~1 day) observed at pharmacologically active doses. Specifically, target-mediated drug disposition (TMDD), commonly observed with monoclonal antibodies (mAb) against membrane-bound receptors (An, 2020), was examined for the role in the PK of Fc-IL-10 fusion proteins. Experiments were conducted to compare the PK of recombinant IL-10 vs those of Fc-fusion proteins. Changes in PK were evaluated in the presence of an IL-10 receptor alpha-blocking mAb and with an Fc-fusion protein that had a reduced receptor binding affinity. Additionally, compartmental

analyses were conducted to quantitatively integrate the PK data. The findings from this work offered insights into the future drug design of using Fc for the  $t_{1/2}$  extension.

## MATERIALS AND METHODS

**Materials and Reagents.** Mouse IL-10 (mIL-10), human IL-10 (hIL-10), mouse Fc-mouse IL-10 (mFc-mIL-10), human Fc-human IL-10 (hFc-hIL-10), and hFc-hIL-10 mutant (hFc-hIL-10 mutant) were produced at Bristol Myers Squibb. Recombinant human IL-10 receptor alpha protein, biotinylated mouse anti-human immunoglobulin G (IgG) Fc mAb, and mouse anti-mouse PD-1 (mPD-1) IgG1 mAb with a single amino acid substitution of aspartic acid to alanine at codon 265 (D265A) were also generated at Bristol Myers Squibb. Recombinant mouse IL-10 receptor alpha protein was obtained from R&D systems (Minneapolis, MN). Rat anti-mouse IL-10 biotinylated antibody, rat anti-human IL-10 antibody, and goat anti-mouse IgG antibody labeled with Alexa Fluor 647 were purchased from Southern Biotech (Birmingham, AL). Rat anti-mIL-10 receptor alpha mAb 1B1.3A was obtained from Bio X Cell (Lebanon, NH). All other reagents were obtained from commercial sources in analytical grade.

### In Vitro Studies

**Determination of Binding Affinity.** The binding affinity, measured as the equilibrium dissociation constant ( $K_d$ ), was determined using a surface plasmon resonance (SPR) method. For the IL-10 receptor alpha  $K_d$  determination, the experiments were conducted using the Biacore™ T200 biosensor system (Cytiva, Marlborough, MA) at 25°C in a buffer (pH 7.2) containing 10 mM  $\text{NaH}_2\text{PO}_4$ , 130 mM NaCl, and 0.05% Tween 20 (PBS-T). The drug molecules (mFc-mIL-10 or hFc-hIL-10) were either directly immobilized on a CM5 chip (Cytiva, Marlborough, MA) using 1-ethyl-3-(3-dimethylaminopropyl)carbodiimide



hydrochloride (EDC) / N-hydroxysuccinimide (NHS) to a density of roughly 300 RUs or captured to a Protein A Series S chip (Cytiva), at 2  $\mu\text{g/mL}$  using 30-second contact time at a flow rate of 10  $\mu\text{L/min}$  to give approximately 200-300 RUs. A mIL-10 receptor alpha solution was prepared in a buffer of 10 mM  $\text{NaH}_2\text{PO}_4$ , 130 mM NaCl, and 0.05% Tween 20 at concentrations of 0.82, 2.5, 7.4, 22.2, 66.6, and 200 nM. Similarly, an hIL-10 receptor alpha solution was prepared in the same buffer at concentrations of 4.1, 12.3, 37.0, 111, 333, and 1000 nM. Protein solutions were then injected for 3 minutes at a flow rate of 30  $\mu\text{L/min}$  followed by 5 minutes of dissociation using the “high performance” sample injection type in the Biacore T200 Software Method Builder. The immobilized surface was regenerated back to baseline using a 60-second injection of 2M  $\text{MgCl}_2$ , followed by a 60-second injection of 20 mM EDTA. The protein A surface was regenerated back to the baseline using two 15-second injections of a glycine solution at pH 1.5. The  $K_d$  was estimated by a global fitting of the data using either the 1:1 Langmuir binding model or the steady-state affinity model available in the Biacore™ T200 Software.

To determine the neonatal Fc receptor (FcRn)  $K_d$  of hFc-hIL-10, SPR studies were conducted on a Biacore™ 8K biosensor system (Cytiva, Marlborough, MA). A series S CM5 sensor chip was equilibrated with PBS-T pH 7.2 SPR running buffer at 25°C, and then hFc-hIL-10 was immobilized by diluting in acetate pH 4.5 and coupling using standard EDC/NHS chemistry, with ethanolamine blocking. The immobilization level obtained was 330 RU for hFc-hIL-10. After priming the system, the binding of human and mouse FcRn analytes was tested by titrating an increasing concentration series of 19.5, 39.1, 78.1, 156, 313, 625, 1250, 2500, 5000, 10000 nM FcRn in PBS-T pH 6.0, as well as a single 2500 nM FcRn injection in PBS-T pH 7.4 to confirm lack of binding at neutral pH. All binding studies were done with association and dissociation times of 180 s each at a flow rate of 30  $\mu\text{L/min}$ . The immobilized surface was

regenerated back to baseline using 2 X 30s injections of Tris pH8 + 150mM NaCl. The  $K_d$  was estimated by a global fitting of the data using either the 1:1 Langmuir binding model or the steady-state affinity model available in the Biacore™ Insight Evaluation Software.

***Evaluation of Cellular Activity.*** The cellular activity of mFc-mIL-10 and hFc-hIL-10 was evaluated in primary T cells by measuring the phosphorylation of STAT3, a downstream signal of the IL-10 receptor alpha activation. For the mouse assay, splenocytes from C57/BL6 mice were used in the studies. Briefly, spleens pooled from mice were manually dissociated and made into single-cell suspension by mechanical disruption and filtering through a 70- $\mu$ M filter followed by red blood cell lysis for 3 minutes at 37°C. Following lysis, cells were washed with phosphate-buffered saline (PBS) (Thermo Fisher Scientific, Waltham, MA), re-suspended in complete media (Roswell Park Memorial Institute 1640, 10% fetal bovine serum, and 0.05 mM 2-mercaptoethanol) and plated at  $5 \times 10^5$  cells per well in a 96-well plate. After a 1-hour rest, mFc-mIL-10 or controls were added to the wells and incubated for 15 minutes at 5% CO<sub>2</sub> at 37°C. The stimulation was stopped using cold fluorescent-activated cell sorting (FACS) buffer (0.5% fetal bovine serum in PBS), cells were washed with FACS buffer, and fixed using BD Cytofix (BD Biosciences, Franklin Lakes, NJ) on ice for 20 minutes before re-suspension in cold Phosflow Perm Buffer III (BD Biosciences, Franklin Lakes, NJ). Samples were subsequently stored at -20°C until staining. After overnight incubation at -20°C, samples were washed twice with FACS buffer and re-suspended in 100  $\mu$ L FACS buffer. Aliquots of samples in 50  $\mu$ L were transferred to 96-well U-Bottom plates and treated with a blocking reagent (BD mouse FC block, BD Biosciences, Franklin Lakes, NJ) at room temperature for 10 minutes, followed by incubation with antibodies for surface and internal markers. For CD3, fluorescein isothiocyanate (FITC)-labeled anti-mouse CD3 antibody (BD Biosciences, Franklin Lakes, NJ) was used. For

pSTAT3, a mouse anti-STAT3-PE (pY705) antibody (BD Biosciences Franklin Lakes, NJ) was employed. After a 30-minute incubation at room temperature, samples were washed twice with 200  $\mu$ L FACS buffer, centrifuged at 1500 rpm for 5 minutes, and re-suspended in 150  $\mu$ L FACS buffer. The samples were then analyzed by a FACSCanto™ X-20 flow cytometer (BD Biosciences Franklin Lakes, NJ).

For the human assay, whole blood obtained from human healthy donors (N = 3) was used in the experiments. Whole blood samples were drawn in heparin tubes and rested for 1 hour at 37°C in 5% CO<sub>2</sub>. hFc-hIL-10 or controls were added to 100  $\mu$ L of blood in 96-well plates and incubated for 15 minutes with 5% CO<sub>2</sub> at 37°C. After incubation, 1.7 mL of Phosflow Lyse/Fix buffer (BD Biosciences Franklin Lakes, NJ) was added to each sample and incubated for 10 minutes at 37°C to fix lymphocytes and lyse red blood cells. Cells were washed one time in FACS buffer and stained for CD3 using an allophycocyanin-labeled anti-CD3 antibody (BioLegend, San Diego, CA) and washed again in FACS buffer before resuspension in 1 mL of cold Phosflow Perm Buffer III (BD Biosciences Franklin Lakes, NJ). Samples were subsequently stored at -20°C. After overnight incubation at -20°C, samples were washed twice with FACS buffer and re-suspended in 100  $\mu$ L FACS buffer. Samples were then stained with antibodies for pSTAT3 using the mouse anti-STAT3-PE (pY705) antibody. After a 30-minute incubation at room temperature, samples were washed twice with 200  $\mu$ L FACS buffer, centrifuged at 1500 rpm for 5 minutes, and re-suspended in 150  $\mu$ L FACS buffer. The samples were then analyzed by the FACSCanto™ X-20 flow cytometer.

**In Vivo Studies.** All studies were conducted according to the study protocols approved by the Bristol Myers Squibb Institutional Animal Care and Use Committee. Animals were acclimated for 7-17 days before the studies and had free access to food and water ad libitum. Female mice

were used in antitumor efficacy studies for practical and compassionate reasons because they are easier to handle than male mice and can be housed together. Additionally, gender differences in immune responses were reported in the literature (Ray et al., 2020). Having mice of the same sex reduced study variability. Consistent with efficacy evaluations, PK studies were also performed in the same gender of mice.

***Exposure to mFc-mIL-10 in efficacy evaluations.*** Systemic exposure to mFc-mIL-10 was evaluated from several efficacy studies conducted in the mouse MC38 and CT26 syngeneic tumor models. Tumor cells (1 million) suspended in sterile Hanks' balanced salt solution were subcutaneously implanted on the right flank of animals. Dosing was initiated typically 7 days after reaching a mean tumor volume of 100 mm<sup>3</sup> and randomization of animals into treatment groups. Mice were weighed immediately after randomization (before administration of treatment) and at least twice weekly through Day 28. The measurement of tumor volume throughout the study was determined by a caliper and recorded twice weekly until all tumors reached either tumor burden or had completely regressed. Tumor burden was identified as a tumor reaching or exceeding 1000 mm<sup>3</sup> for two consecutive measurements, or exceeding 2000 mm<sup>3</sup> at any one measurement. Animals that had their tumor completely regressed were palpated weekly to confirm tumor rejection.

mFc-mIL-10 was evaluated as a single agent for antitumor efficacy in the mouse MC38 syngeneic tumor model (female C57BL6 mice, ~20 g, Charles River Laboratories, Wilmington, MA). Two efficacy studies were conducted. The drug was formulated in phosphate-buffered saline (PBS) and given as a single dose intraperitoneally (IP) to mice at a dosing volume of 10 mL/kg. The doses studied were 0.1, 0.3, 1, 3, and 10 mg/kg, with 10 mice per dose group along with an isotype control group. In one of the efficacy studies, systemic exposure to mFc-mIL-10

was obtained from tumor-bearing mice, in which serial blood samples of 60  $\mu$ L were obtained via submandibular bleeds at 4 and 168 hours after the dose, with 5 mice per time point. Submandibular bleeds were performed with the use of a sterile 5-mm Goldenrod animal lancet (Braintree Scientific Inc., Braintree, MA). Animals were briefly restrained and an applicable volume of blood was collected from a puncture made proximal of the mandibular bone where the submandibular vein and the facial vein converge. Additionally, as part of the efficacy experiment, a dedicated PK evaluation with mFc-mIL-10 was conducted in the satellite groups of non-tumor-bearing mice at the doses of 0.3 and 3 mg/kg IP, in which blood samples (60  $\mu$ L) were harvested via submandibular bleeds at 1, 5, 24, 72, 168, 240, and 336 hours post-dose in a composite fashion, with 3 mice per time point. After the blood sample collection at each time point, serum samples were harvested and stored at  $\leq -70^{\circ}\text{C}$  until sample analysis for mFc-mIL-10 concentrations.

In the mouse CT26 syngeneic tumor model (female BALB/c mice,  $\sim 20$  g, Envigo, Indianapolis, IN), the antitumor efficacy of mFc-mIL-10 was evaluated in combination with a mouse anti-mPD-1 mAb in three experiments. The anti-mPD-1 mAb was administered every 4 days at 10 mg/kg IP for 3 doses, while mFc-mIL-10 was given as a single IP injection. The doses of mFc-mIL-10 in the first study were 0.1, 0.3, and 1 mg/kg. They were 0.1 and 0.3 mg/kg in the second study and 0.03, 0.1, and 0.3 mg/kg in the third study. Eight or ten mice were studied at each dose level along with isotype control and an anti-mPD-1 monotherapy group. Blood samples (10  $\mu$ L) were obtained compositely in the first study and serially in the second and third studies. They were collected by microsampling on the tail vein from tumor-bearing mice at 4, 24, 48, 96, 168, 192 (or 216), 336, and 504 hours post-dose, with 4 or 6 mice per time point. After the blood sample collections at each time point, they were diluted with 90  $\mu$ L Rextip A buffer

(Gyros AB, Uppsala, Sweden) and stored at  $\leq -70^{\circ}\text{C}$  until sample analysis for mFc-mIL-10 concentrations.

***Intravenous pharmacokinetic studies with mFc-mIL-10 and hFc-hIL-10.*** Pharmacokinetic studies were conducted in non-fasted female C57BL6 mice (20-25 g, Charles River Laboratories, Wilmington, MA) after intravenous (IV) administration at the doses of 0.05, 0.5, and 5 mg/kg. At each dose, four mice received either mFc-mIL-10 or hFc-hIL-10 that was formulated in PBS at a dosing volume of 5 mL/kg. Serial blood samples (10  $\mu\text{L}$ ) were obtained by microsampling on the tail vein at predose, 0.05, 1, 3, 5, 7, 24, 48, 72, 96, 168, 240 hours post-dose and diluted with 90  $\mu\text{L}$  Rxxip A buffer. At the end of the studies, serum samples (30-50  $\mu\text{L}$ ) were also collected via cardiac puncture. Samples were stored at  $\leq -70^{\circ}\text{C}$  until analysis for mFc-mIL-10 or hFc-hIL-10 concentrations.

***Intravenous pharmacokinetic studies with mIL-10 and hIL-10.*** Pharmacokinetic studies were conducted in non-fasted female C57BL6 mice (20-25 g, Charles River Laboratories, Wilmington, MA) after IV administration at the doses of 0.05, 0.5, and 5 mg/kg. At each dose, four mice received either mIL-10 or hIL-10 that was formulated in PBS at a dosing volume of 5 mL/kg. Serial blood samples (10  $\mu\text{L}$ ) were harvested by microsampling on the tail vein at predose, 0.05, 0.5, 1, 5, 7, and 24 hours post-dose and diluted with 90  $\mu\text{L}$  Rxxip A buffer. At the end of the studies, serum samples (30-50  $\mu\text{L}$ ) were also collected via cardiac puncture. Samples were stored at  $\leq -70^{\circ}\text{C}$  until analysis for mIL-10 or hIL-10 concentrations.

***Intraperitoneal pharmacokinetic study with mFc-mIL-10 in the presence and absence of a goat anti-mIL-10 receptor alpha antibody.*** Non-fasted female BALB/c mice (20-25 g, Charles River Laboratories, Wilmington, MA) were used in the study. The goat anti-mIL-10 receptor

alpha antibody was administered subcutaneously (SC) one day before the dosing of mFc-mIL-10. The intended doses for the anti-mIL-10 receptor alpha antibody were 5 and 50 mg/kg. Due to a limited quantity of the dosing solutions, two mice in the 5-mg/kg group received the full dose, while the third mouse was given a dose of 3.5 mg/kg. In the 50-mg/kg group, two mice received the full dose, and the third mouse was dosed at 13 mg/kg. Additionally, PBS as the vehicle for the anti-mIL-10 receptor alpha antibody was given to four mice as the control group. One day after the SC administration of the anti-mIL-10 receptor alpha antibody, mFc-mIL-10 formulated in PBS was administered intraperitoneally at a dose of 0.1 mg/kg, with a dosing volume of 5 mL/kg. Serial blood samples (10  $\mu$ L) were obtained by microsampling on the tail vein at predose, 4, 24, 48, 72, 79, 144, and 168 hours post-dose and diluted with 90  $\mu$ L Rxxip A buffer. At the end study, serum samples (30-50  $\mu$ L) were also collected via cardiac puncture. Samples were stored at  $\leq -70^{\circ}\text{C}$  until analysis for mFc-mIL-10 concentrations.

***Intraperitoneal pharmacokinetic studies with hFc-hIL-10 and hFc-hIL-10 mutant.*** hFc-hIL-10 or hFc-hIL-10 mutant, formulated in PBS at a dosing volume of 5 mL/kg, was given to 4 non-fasted female BALB/c mice (20-25 g, Charles River Laboratories, Wilmington, MA) at a dose of 0.1 mg/kg. Serial blood samples (10  $\mu$ L) were collected by microsampling on the tail vein at predose, 4, 24, 48, 72, 79, 144, and 168 hours post-dose and diluted with 90  $\mu$ L Rxxip A buffer. At the end study, serum samples (30-50  $\mu$ L) were also collected via cardiac puncture. Samples were stored at  $\leq -70^{\circ}\text{C}$  until analysis for hFc-hIL-10 and hFc-hIL-10 mutant concentrations.

## **Sample Analysis.**

***Quantitation of mFc-mIL-10.*** The concentrations of mFc-mIL-10 in mouse samples (10% blood in Rxxip A buffer or serum) were measured using a microfluidic fluorescence immunoassay on

a Gyrolab™ xP Workstation (Gyros AB, Uppsala, Sweden). A biotinylated rat anti-mIL-10 antibody (Southern Biotech, Birmingham, AL) was used as the capture reagent, and a goat anti-mIgG antibody labeled with Alexa Fluor 647 (Southern Biotech, Birmingham, AL) was used as the detection reagent. For diluted blood samples (10% blood in Rxxip A buffer), standard curves and quality control (QC) samples defining the dynamic range of the bioanalytical method were prepared in the 10% mouse blood with Rxxip A buffer and processed in the same fashion as the test samples. For serum samples, they were analyzed at 5-fold dilution in PBS with 1% BSA and 1M sodium chloride; the corresponding standard and QC samples were prepared in the same way as the serum test samples. Aliquots of diluted test samples, QC samples, standards, and reagents were added to 96-well polymerase chain reaction (PCR) microplates (Thermo Scientific, Cambridge, MA). The Gyrolab workstation transferred samples and reagents from the microplates to each of the microstructures within a Gyrolab Bioaffy compact disc (CD) and spun each CD at the optimized speed and time controlled by the Gyros software to ensure uniform optimal reaction times throughout the integrated assay workflow. All assay steps were automated and controlled by the Gyros control software. The mFc-mIL-10 concentrations in the test samples were quantified by a log-log linear-fit regression model using the SoftMax Pro software (Molecular Devices, Sunnyvale, California). Standard curves and QC samples were evaluated using target acceptance criteria for inaccuracy and imprecision of  $\pm 20\%$  of the nominal concentration to be considered acceptable for assay performance. The lower limit of quantitation (LLOQ) in diluted blood and serum samples were 0.4 and 3 ng/mL (0.004 and 0.03 nM), respectively. The LLOQ in plasma after the conversion of drug concentrations from diluted blood samples using a theoretical dilution factor of 17.36 (see Data Analysis for details) was 6.9 ng/mL (0.08 nM).



***Quantitation of hFc-hIL-10 and hFc-hIL-10 mutant.*** The concentrations of hFc-hIL-10 and hFc-hIL-10 mutant in mouse samples (10% blood in Rxxip A buffer or serum) were measured using a chemiluminescence immunoassay platform developed at Bristol Myers Squibb. A rat anti-hIL10 (Southern Biotech, Birmingham, AL) and biotin-labeled mouse anti-human IgG Fc antibody (produced at Bristol Myers Squibb) were used as the capture and detection reagents, respectively. For diluted blood samples (10% blood in Rxxip A buffer), standard curves and QC samples defining the dynamic range of the bioanalytical method were prepared in the 10% mouse blood with Rxxip A buffer and processed in the same fashion as the test samples. Serum samples were analyzed in Rxxip buffer A and loaded in the capture reagent coated, blocked 96-well flat-bottom Nunc MaxiSorp black plate (Thermo Fisher Scientific, Waltham, MA). After the incubation and wash step, the detection reagent, an in-house biotin-labeled mouse anti-human IgG Fc antibody was added. Followed by another incubation and wash steps NeutrAvidin-HRP (Thermo Fisher Scientific, Waltham, MA) was added. After the final incubation and wash step, Pico substrate solution (Thermo Fisher Scientific, Waltham, MA) was added to assay plates and read in SpectraMax plate reader at the luminescence mode. Calibrators and QCs were analyzed on each assay plate along with samples to ensure acceptable assay performance. The concentrations of hFc-hIL-10 or hFc-hIL-10 mutant in mouse serum samples were calculated from the luminescence intensity using a log-log linear calibration curve. Assay performance was within the acceptable range: % CV of the standards and QC was below 20 %, and QC recovery was within  $\pm 20$  % of the nominal values. The LLOQ of hFc-hIL-10 in diluted blood and serum samples were 0.4 and 1 ng/mL (0.004 and 0.01 nM), respectively. The corresponding LLOQ in plasma after the conversion of drug concentrations from diluted blood samples using the theoretical dilution factor of 17.36 (see Data Analysis for details) was 6.9 ng/mL (0.08 nM). The

LLOQ of the hFc-hIL-10 mutant in diluted blood and serum samples were 2.5 and 2.5 ng/mL (0.03 nM), respectively. The corresponding LLOQ of the hFc-hIL-10 mutant in plasma after the correction from diluted blood samples was 43 ng/mL (0.5 nM).

***Quantitation of mIL-10.*** The concentrations of mIL-10 in mouse samples (10% blood in REXXIP A buffer or serum) were measured using the same procedure as described above for mFc-mIL-10, except that a rat anti-mIL-10 antibody labeled with Alexa Fluor 647 (Southern Biotech, Birmingham, AL) was used as the detection reagent. The LLOQ in diluted blood and serum samples were 0.025 and 1 ng/mL (0.0007 and 0.03 nM), respectively. The corresponding LLOQ in plasma after the correction from diluted blood samples was 0.4 ng/mL (0.01 nM).

***Quantitation of hIL-10.*** The concentrations of hIL-10 in mouse samples (10% blood in REXXIP A buffer or serum) were measured using the same procedure as described above for mFc-mIL-10, except that a biotinylated rat anti-hIL-10 antibody (Southern Biotech, Birmingham, AL) and a rat anti-hIL-10 antibody labeled with Alexa Fluor 647 (Southern Biotech, Birmingham, AL) were used as the capture and detection reagents, respectively. The LLOQ in diluted blood and serum samples were 0.25 and 0.25 ng/mL (0.007 nM), respectively. The corresponding LLOQ in plasma after the correction from diluted blood samples was 4 ng/mL (0.1 nM).

## **Data Analysis.**

Data are expressed as mean  $\pm$  standard deviation (SD). For REXXIP A buffer-diluted blood samples collected in mice, a theoretical dilution factor of 17.36 was used for correcting the drug levels to undiluted plasma drug concentrations (Joyce et al., 2014). The theoretical dilution factor was determined by assuming the biotherapeutic agents such as recombinant IL-10 and associated Fc-fusion proteins largely reside in the plasma volume. A dilution of 10  $\mu$ L of blood

into 90  $\mu\text{L}$  Rxxip A buffer dilutes the drugs residing in 5.5  $\mu\text{L}$  of plasma water, assuming a hematocrit value of 0.45. As a result, the theoretical dilution factor is calculated as the sum of 90  $\mu\text{L}$  buffers and 5.5  $\mu\text{L}$  plasma water divided by 5.5  $\mu\text{L}$  plasma water ( $95.5 \div 5.5 = 17.36$ ).

**Noncompartmental pharmacokinetic analysis.** The pharmacokinetic parameters were obtained by noncompartmental analysis of plasma concentration vs time data using PKSolver (Zhang et al., 2010). The peak concentration ( $C_{\text{max}}$ ) and time for  $C_{\text{max}}$  ( $T_{\text{max}}$ ) were recorded directly from experimental observations. The area under the curve from time zero to infinity ( $\text{AUC}_{\text{tot}}$ ) was calculated using a combination of linear and log trapezoidal summations. The total plasma clearance ( $\text{CL}_{\text{tot}}$ ), steady-state volume of distribution ( $V_{\text{ss}}$ ), and terminal  $t_{1/2}$  were estimated after IV administration.

**Compartmental pharmacokinetic analysis.** The IV PK data were fitted with a 2-compartment model. To fit the mFc-mIL-10 and hFc-hIL-10 data, target- and non-target-mediated elimination were incorporated into the 2-compartment model. The differential equations are shown below:

$$V_c \frac{dC_p}{dt} = A_{\text{peripheral}} \times k_{21} - \left( k_{\text{el,non-target-mediated}} + k_{12} + \frac{V_{\text{max,target-mediated}}}{K_m \times V_c + V_c \times C_p} \right) \times V_c \times C_p \quad (1)$$

$$\frac{dA_{\text{peripheral}}}{dt} = k_{12} \times V_c \times C_p - k_{21} \times A_{\text{peripheral}} \quad (2)$$

where  $A_{\text{peripheral}}$  is the drug amount in the peripheral compartment;  $C_p$  is the drug concentration in the central compartment;  $V_c$  is the volume of distribution in the central compartment;  $k_{12}$  and  $k_{21}$  are the transfer rate constants between the central and peripheral compartment;  $k_{\text{el,non-target-mediated}}$  is the non-target-mediated first-order elimination rate constant;  $V_{\text{max,target-mediated}}$  is the maximum

elimination rate mediated by a target;  $K_m$  is the binding affinity to the target. For mIL-10 and hIL-10, only non-target-mediated elimination was needed to fit the IV PK data. With Equation 2 remaining the same, Equation 1 becomes:

$$V_c \frac{dC_p}{dt} = A_{\text{peripheral}} \times k_{21} - (k_{\text{el,non-target-mediated}} + k_{12}) \times V_c \times C_p \quad (3)$$

At time zero, the following initial condition exists for IV administration.

$$C_{p,t=0} = \frac{Dose_{IV}}{V_c}$$

$$A_{\text{peripheral},t=0} = 0$$

where  $Dose_{IV}$  is the IV dose administered. It is worth noting that it was necessary to consider non-specific drug adsorption to devices during dosing solution preparations and actual dosing at the low IV dose of 0.05 mg/kg. Otherwise, the concentrations at 0.05 mg/kg predicted by the PK model were consistently higher than the observed values. In contrast, the phenomenon was not evident at two higher doses of 0.5 and 5 mg/kg. As a result, the initial condition for  $C_{p,t=0}$  at 0.05 mg/kg was equal to:

$$C_{p,t=0, \text{at } 0.05 \text{ mg/kg}} = \frac{Dose_{IV} \times \% \text{remaining}}{V_c}$$

where %remaining is the percentage of the dose remaining after nonspecific drug adsorption and the value was estimated from the PK model.

To model the mFc-mIL-10 IP PK data, the first-order absorption coupled with the 2-compartment model was employed. The differential equations are given below:

$$\frac{dA_{IP}}{dt} = -k_a \times A_{IP} \quad (4)$$

$$V_{c,apparent} \frac{dC_p}{dt} = k_a \times A_{IP} + A_{peripheral} \times k_{21} - \left( k_{el,non-target-mediated} + k_{12} + \frac{V_{max,target-mediated}}{K_m \times V_{c,apparent} + V_{c,apparent} \times C_p} \right) \times V_{c,apparent} \times C_p \quad (5)$$

$$\frac{dA_{peripheral}}{dt} = k_{12} \times V_{c,apparent} \times C_p - k_{21} \times A_{peripheral} \quad (6)$$

where  $A_{IP}$  is the amount of the drug at the IP absorption site,  $k_a$  is the absorption rate constant, and  $V_{c,apparent}$  is the apparent volume of distribution in the central compartment after IP administration. In this case, the  $V_{c,apparent}$ , as opposed to the IP bioavailability, was used as a parameter to model the data after IP administration. It was because the IP bioavailability estimated from the simultaneous fitting of the mFc-mIL-10 IV and IP data was >100% across a wide dose range (0.03 - 3 mg/kg), indicating a systematic difference between the IV and IP studies. Therefore, the  $V_{c,apparent}$  was used as a scalar to fit the IP data and avoid the wrong impression that the IP bioavailability of mFc-mIL-10 was >100%.

At time zero, the following conditions exist:

$$A_{IP,t=0} = Dose_{IP}$$

$$C_{P,t=0} = 0$$

$$A_{Peripheral,t=0} = 0$$

where  $Dose_{IP}$  is the dose administered via the IP route. Same as the IV PK data modeling, the non-specific drug adsorption to devices needed to be considered for the low IP dose of 0.03

mg/kg but not for higher doses. Consequently, the initial condition for  $A_{IP,t=0}$  at the 0.03-mg/kg IP dose was equal to:

$$A_{IP,t=0,at\ 0.03\ mg/kg} = Dose_{IP} \times \%remaining$$

For the mFc-mIL-10 IP PK data, they were simultaneously fitted together with the IV data to obtain one set of parameters except for  $V_c$ ,  $V_{c,apparent}$ , and  $k_a$ .

The compartmental PK analysis was conducted using SAAM II (v2.3.1.1, The Epsilon Group, Charlottesville, VA) to describe the average PK data across the dose range evaluated. The weighting function was  $1/y$ . The goodness of fit was assessed by the minimization of the objective function, Akaike and Schwarz-Bayesian information criteria, visual inspection of the fitting and residual plots, and the precision of the parameters estimated.

**Statistical analysis.** The Student's t-test was used. A difference was considered significant when the p-value was  $<0.05$ .

## RESULTS

### Properties of mFc-mIL-10 and hFc-hIL-10

Table 1 summarizes the various properties of mFc-mIL-10 and hFc-hIL-10, with the sequence structures and additional characterization information available in Supplemental Data. The molecular weights of both molecules were about 90 kDa, and they had a comparable binding affinity  $K_d$  ( $\sim 3$  nM) to mIL-10 receptor alpha. The  $K_d$  of hFc-hIL-10 towards hIL-10 receptor alpha was 0.6 nM, comparable to that (0.05 - 0.5 nM) of hIL-10 reported in the literature (Moore et al., 2001; Walter, 2014). The cellular activity in mouse and human CD3<sup>+</sup> T cells was also in

the same range for both agents (Table 1). These results confirm that hFc-hIL-10 cross-reacts to mIL-10 receptor alpha.

mFc-mIL-10 had the Fc domain of IgG1 with a single amino acid substitution of aspartic acid to alanine at codon 265 (D265A). The  $K_d$  of mFc-mIL-10 to the mouse neonatal Fc receptor (FcRn) was previously reported to be 640 nM (Wang et al., 2020). In comparison, hFc-hIL-10 carried the Fc domain of human IgG1 with 3 amino acid substitutions (L234A, L235E, and G237A) to reduce the effector function. The  $K_d$  of hFc-hIL-10 to the mouse and human FcRn was determined to be 200 and 1,100 nM, respectively (Table 1). The results are consistent with the literature findings in which human IgG antibodies are found to have a tighter binding affinity to mouse FcRn than to humans (Abdiche et al., 2015).

### **Systemic Exposure to mFc-mIL-10 after Intraperitoneal Administration in Efficacy Evaluations**

mFc-mIL-10 was pharmacologically active in the mouse syngeneic models after a single IP dose injection. In the MC38 mouse tumor model, the percentage of mice that were tumor-free at the doses of 0.1, 0.3, 1, 3, and 10 mg/kg, averaged from two antitumor efficacy studies, was 5, 65, 95, 90, and 90%, respectively. In the CT26 mouse tumor model, mFc-mIL-10 was efficacious when combined with an anti-mPD-1 mouse surrogate; the percentage of mice without tumors at the doses of 0.03, 0.1, 0.3, and 1 mg/kg averaged from three studies was 40, 77, 85, and 100%, respectively, compared with 14% of animals receiving only the anti-mPD-1 mAb. These data indicate that mFc-mIL-10 was pharmacologically active at doses of  $\geq 0.1$  mg/kg.

In the efficacy studies, the systemic exposure to mFc-mIL-10 after IP administration was also examined. Figure 2a shows the plasma concentration-time profiles of mFc-mIL-10 at the dose

range of 0.03 - 3 mg/kg. With a nominal dose ratio of 1:3:10:33:100 and a nonspecific adsorption-corrected dose ratio of 1:8.8:26:88:263, the  $C_{\max}$  and  $AUC_{\text{tot}}$  ratios were 1:11:46:189:556 and 1:14:56:283:937, respectively (Table 2). The terminal  $t_{1/2}$  also increased with the doses. Moreover, at the pharmacologically active doses of 0.1 - 0.3 mg/kg, the terminal  $t_{1/2}$  was 1.2 - 1.5 days, significantly shorter than typical mouse IgG1  $t_{1/2}$  of 6-8 days (Vieira and Rajewsky, 1988).



## **mFc-mIL-10 and hFc-hIL-10 Pharmacokinetics after Intravenous Administration to Mice**

To investigate the nonlinear PK observed in the efficacy evaluations after IP dosing, mFc-mIL-10 and hFc-hIL-10 were administered intravenously to non-tumor-bearing mice at the doses of 0.05, 0.5, and 5 mg/kg. Table 3 summarizes the PK parameters of mFc-mIL-10 and hFc-hIL-10 estimated using noncompartmental analysis. Figures 2b and 2c depict the plasma concentration-time profiles after IV administration. Similar to the results from the IP dosing, mFc-mIL-10 exhibited a significant nonlinear PK after IV administration. With a nominal dose ratio of 1:10:100 and a nonspecific adsorption-corrected dose ratio of 1:28:278, the  $C_{\max}$  and  $AUC_{\text{tot}}$  ratios were 1:28:263 and 1:181:1830, respectively (Table 3). The  $CL_{\text{tot}}$  decreased from 239 to 33 mL/d/kg when the dose increased from 0.05 to 5 mg/kg. These clearance values appear to be higher than the clearance data ( $\sim 10$  mL/d/kg) commonly observed with mAb in mice without TMDD (Betts et al., 2018). The  $V_{\text{ss}}$  showed an increasing trend with the dose but was still in a range comparable to the values ( $\sim 60$ -130 mL/kg, Betts et al., 2018) of mAb which has a larger molecular weight than that of mFc-mIL-10. Because of dose-dependent changes in the  $CL_{\text{tot}}$  and  $V_{\text{ss}}$ , the terminal  $t_{1/2}$  values at 0.05, 0.5, and 5 mg/kg were 0.22, 2.6, and 3.9 days, respectively. These results indicate that the disposition of mFc-mIL-10 was nonlinear.

Like mFc-mIL-10, hFc-hIL-10 exhibited a nonlinear PK after IV administration. With a nominal dose ratio of 1:10:100 and a nonspecific adsorption-corrected dose ratio of 1:19:192, the  $C_{\max}$  and  $AUC_{\text{tot}}$  ratios were 1:21:187 and 1:75:633, respectively (Table 3). The  $CL_{\text{tot}}$  decreased with the dose (162 to 41 mL/d/kg), with the  $V_{\text{ss}}$  showing a slightly increasing trend (106 to 161 mL/kg). As a result, the terminal  $t_{1/2}$  at 0.05, 0.5, and 5 mg/kg was 0.45, 2.5, and 2.0 days, respectively. Similar findings between mFc-mIL-10 and hFc-hIL-10 pointed to the direction of

TMDD as the cause of nonlinear PK, because both molecules had similar binding affinity values to mIL-10 receptor alpha (Table 1).

### **mIL-10 and hIL-10 Pharmacokinetics after Intravenous Administration to Mice**

To examine the role of the target in the nonlinear PK observed with Fc-fusion proteins, the PK of mIL-10 and hIL-10 was studied in non-tumor-bearing mice following IV administration. Figure 3 shows the plasma concentration-time profiles of mIL-10 and hIL-10 at the doses of 0.05, 0.5, and 5 mg/kg, with the PK parameters summarized in Table 4. In contrast to the nonlinear PK observed with the Fc-fusion proteins, mIL-10 and hIL-10 demonstrated linear PK after IV administration. Across the same dose range as that of the Fc-fusion proteins, the  $CL_{tot}$  and  $V_{ss}$  were largely dose-independent (Table 3). The  $CL_{tot}$  of mIL-10 was similar to the value reported in the literature (Alvarez et al., 2012), while the  $CL_{tot}$  of hIL-10 was about 2-fold higher than that of mIL-10. The  $V_{ss}$  of mIL-10 and hIL-10 was in a range of 103-143 mL/kg and 77-207 mL/kg, respectively. These values are generally in line with the literature data (Huhn et al., 1996; Alvarez et al., 2012). The terminal  $t_{1/2}$  was 1-1.5 hours, consistent with the expected  $t_{1/2}$  values for cytokines. These data suggest that the cytokine PK behaved differently from that of the Fc-fusion proteins.

### **Compartmental Analysis of Pharmacokinetic Data of Fc-fusion Proteins and Cytokines in Mice**

To further gain insight into the PK behaviors of Fc-fusion proteins and their corresponding cytokines, compartmental analysis was conducted. Table 5 summarizes the estimated PK parameters, with model-fitted curves displayed in Figures 2 and 3. For each molecule, the PK model, developed using one set of parameters, described the central tendency of the data across a

wide dose range. The key models tested and testing performance measured as the objective function, Akaike information criterion, Schwarz-Bayesian information criterion are shown in Supplemental Tables 1-4, with diagnostic plots displayed in Supplemental Figures 1-4.

For mFc-mIL-10, the IV and IP data were simultaneously fitted. Because a systematic difference in drug concentrations was observed between the IV and IP routes, the  $V_{c,apparent}$  as opposed to the IP bioavailability was used as a scalar to account for the apparent difference between the two routes of administration. The  $V_c$  after IV administration was estimated to be 35 - 81 mL/kg, while the  $V_{c,apparent}$  after IP administration of mFc-mIL-10 was 45 mL/kg. The  $V_c$  values were comparable to what was reported for mAb (Betts et al., 2018).

For the elimination of Fc-fusion protein, TMDD was assumed in the PK model, and the Michaelis-Menten kinetics was used. The in vitro binding affinity to the mIL-10 or hIL-10 receptor alpha was used as the  $K_{m,target-mediated}$  for the curve fitting. Using this approach, nonlinear PK associated with the Fc-fusion proteins was reasonably described. The  $k_{el,non-target-mediated}$  for mFc-mIL-10 and hFc-hIL-10 was 0.022 and 0.023 hours<sup>-1</sup>, respectively, suggesting that differences in the FcRn  $K_d$  (640 vs. 200 nM) between mFc-mIL-10 and hFc-hIL-10 did not result in differences in the non-targeted-mediated clearances. Based on these values, the  $t_{1/2}$  for non-targeted mediated pathways, calculated as  $0.693/k_{el,non-target-mediated}$ , was ~30 hours, which is in line with the mouse  $t_{1/2}$  (17 hours) observed with elastin-like polypeptides that had an MW of 86 kDa (Kuna et al., 2018).

For recombinant IL-10 proteins, incorporating TMDD into the cytokine elimination did not improve the data fitting. A 2-compartment PK model without TMDD was sufficient to explain the data (Supplemental Figures 3 and 4, Supplemental Tables 3 and 4). The  $k_{el,non-target-mediated}$

estimated for mIL-10 and hIL-10 was 4.3 and 5.9 hours<sup>-1</sup>, respectively. The corresponding CL<sub>tot</sub> predicted from the PK model was 2.5 and 5.7 mL/min/kg, respectively. These clearance values are in the same order of magnitude as the glomerular filtration rate (14 mL/min/kg) in mice (Davies and Morris, 1993). Additionally, the terminal t<sub>1/2</sub> of mIL-10 and hIL-10 predicted from the PK model was 1.1 and 0.9 hours, respectively. The values are shorter than the mouse t<sub>1/2</sub> (4.7 hours) reported for elastin-like polypeptides that had the same molecular weight (37 kDa) as that of IL-10 (Kuna et al., 2018). It is possible that TMDD still exists for the cytokines but cannot be manifested readily due to a high non-targeted-mediated clearance such as renal filtration.

## **mFc-mIL-10 Intraperitoneal Pharmacokinetics in Presence and Absence of Goat Anti-mIL-10 Receptor Alpha Antibody**

To illustrate the role of TMDD in the PK of Fc-fusion proteins, the PK of mFc-mIL-10 was evaluated in the presence and absence of a goat anti-mIL-10 receptor alpha antibody. The plasma concentration-time profiles of mFc-mIL-10 are shown in Figure 4a, with different doses of the anti-mIL-10 receptor alpha given subcutaneously 1 day before the dosing of mFc-mIL-10. In the absence of the receptor-blocking antibody, the mFc-mIL-10 curve reproduced the IP plasma concentration-time profile observed at the same dose in efficacy evaluations. In the presence of the receptor-blocking antibody, the mFc-mIL-10 plasma concentrations did not decline; rather they went up over time in a manner that is consistent with the doses of the receptor-blocking antibody. Figure 4b shows a significant correlation ( $p < 0.05$ ) between the  $AUC_{tot}$  of mFc-mIL-10 and the dose of the receptor-blocking antibody. The rising concentrations of mFc-mIL-10 over time are presumably due to the continuous production of the endogenous mIL-10 in the body and the inability of binding to the IL-10 receptor alpha because of the receptor-blocking antibody.

## **hFc-hIL-10 and hFc-hIL-10 Mutant Pharmacokinetics after Intraperitoneal Administration to Mice**

To further provide experimental evidence of the TMDD role in governing the PK of the Fc-fusion proteins, the IP PK of an hFc-hIL-10 mutant was studied side by side with the hFc-hIL-10 in mice. As shown in Table 6, the mutant binding affinity to the mIL-10 receptor alpha was 380-fold weaker than that of hFc-hIL-10. Figure 5 shows that hFc-hIL-10 plasma concentrations declined below the LLOQ value  $\sim 3$  days after IP dosing at 0.1 mg/kg, whereas the mutant drug

levels given at the same dose were well maintained throughout at least 6 days. The terminal  $t_{1/2}$  of hFc-hIL-10 was approximated to be  $0.71 \pm 0.10$  days, significantly different from that ( $1.9 \pm 0.57$  days) of the hFc-hIL-10 mutant ( $p < 0.05$ ). One confounding factor to the data interpretation was that the concentrations of hFc-hIL-10 were consistently lower than those of the hFc-hIL-10 mutant by ~4-fold. The data itself may not sufficiently prove the role of TMDD in PK, but it added evidence to other data.

## DISCUSSION

Fc fusion is an approach commonly employed to extend the  $t_{1/2}$  of peptides, antibody fragments, cytokines, receptor extracellular domains, et al. by increasing the molecular size to reduce the renal filtration and leveraging the FcRn-mediated recycling. Several factors affect the PK of Fc-fusion proteins. These include but are not limited to the degree of glycosylation, binding kinetic differences in the FcRn dissociation between IgG and Fc-fusion proteins, and TMDD (Liu, 2018). In this report, we investigated the PK of Fc-IL-10 fusion proteins and the cause of nonlinear PK observed in mice. Modeling evidence and experimental results were presented to demonstrate the role of TMDD in the PK of Fc-IL-10 fusion proteins at pharmacologically active doses.

Most PK studies presented herein were conducted by the serial sampling of 10  $\mu$ L blood followed by the dilution of 90  $\mu$ L Rexipp buffer. To obtain plasma drug concentrations from diluted blood samples, a theoretical dilution factor of 17.36, reported by Joyce et al. (2014), was used by assuming that the Fc-fusion proteins and IL-10 did not enter red blood cells and a hematocrit value was 0.45. The assumptions above were also supported by the experimental data generated. First, the serum vs. diluted blood concentration ratios of mFc-mIL-10 in matched

samples were  $13.3 \pm 1.9$  (N = 5). Second, following an IP dose of 0.3 mg/kg, the mFc-mIL-10 serum concentration-time profile obtained by composite serum sampling was superimposed to that in plasma after the correction of drug concentrations in diluted blood samples with the theoretical dilution factor (data not shown). Third, the mIL-10 plasma IV PK parameters obtained from the diluted blood samples after the correction with the theoretical dilution factor were in agreement with the values reported in the literature (Alvarez et al., 2012). Based on these pieces of evidence, the use of the theoretical dilution factor of 17.36 to obtain plasma drug concentrations from diluted blood samples was justified.

Non-specific adsorption of cytokines and Fc-fusion proteins to dosing vials and devices sometimes occurs at a low  $\mu\text{g/kg}$  dose range. During the compartmental analysis, when the same central compartment volume of distribution (i.e.,  $V_c$ ) was used across the dose range, it was found that the concentration-time profiles predicted from the PK model consistently over-predicted the observed data at the IV dose of 0.05 mg/kg and the IP dose of 0.03 mg/kg. The over-predictions occurring at the first time point 3 min post an IV bolus dose cannot be explained by TMDD. As a result, the %drug remaining in the dosing solution as a parameter to account for drug loss due to non-specific adsorption was introduced to the PK model at the low doses of 0.03 - 0.05 mg/kg. The approach resulted in a successful data fitting and enabled one set of model parameters to describe the PK data. The need of accounting for non-specific drug adsorption that led to drug losses in dosing solutions was supported by an in vitro experiment, in which an hFc-hIL-10 solution of 0.02 mg/mL (0.1 mg/kg using 5 mL/kg dosing volume) in a dosing syringe was tested at room temperature for 2 hours and only 60% of the drug concentration was recovered afterward.

In this work, the mFc-mIL-10 and hFc-hIL-10  $t_{1/2}$  (2-4 days) at the doses (e.g., 5 mg/kg) that saturated the TMDD appeared to be shorter than the typical IgG in mice. For example, the IgG1  $t_{1/2}$  in mice was reported to be 6-8 days (Vieira and Rajewsky, 1988). In Tg32 hFcRn transgenic mice, the average terminal  $t_{1/2}$  from 11 mAbs was ~10 days (Betts et al., 2018). These findings are consistent with the work done by Unverdorben et al. (2016), where they found that the terminal  $t_{1/2}$  of two Fc fusion proteins in mice at 1 mg/kg was 4.3-4.6 days vs. 9.0-9.3 days for their respective IgG1 antibodies. It is also possible that differences in the glycosylation pattern between IgG and Fc-fusion proteins and inherent instability in Fc-fusion proteins may affect the PK. In our case, PK properties between batches were consistent, suggesting consistent glycosylation patterns in IL-10 Fc-fusion proteins. Additionally, cleavage products in the circulation were examined by LC/MS using intact mass analysis and a peptide-based approach. No evidence of cleavage products was found (data not shown).

Through the investigation, the cause of nonlinear PK associated with IL-10 Fc-fusion proteins was attributed to TMDD, which led to the terminal  $t_{1/2}$  of ~1 day at pharmacologically active doses in mice. Several pieces of evidence support the conclusion. First, IL-10 receptor alpha is widely expressed in hematopoietic cells. Although the basal expression is 100-700 copies per cell (Tan et al., 1993; von Haehling et al., 2015), the sheer volume of hematopoietic cell counts in the body leads to the IL-10 receptor alpha concentration estimated to be in an nM range. For example, the receptor concentrations in the mouse spleen were estimated to be 0.5-1 nM, based on the total lymphocyte counts of  $1.5-2.4 \times 10^8$  (Berzins et al., 1998; Liu et al., 2005), spleen weight of 0.1 g (Davies and Morris, 1993), and 300 receptor copies per lymphocyte. The target levels were in the same range as the concentrations of IL-10 Fc-fusion proteins at 0.03 - 0.05 mg/kg, where TMDD had a profound effect on the PK of these molecules. Second, although IL-



IL-10 binds to glycosaminoglycans, the components of the extracellular matrix in the body, with an affinity of 54 nM (Salek-Ardakani et al., 2000; Künze et al., 2016), binding is a distribution process and cannot explain the nonlinear elimination observed with IL-10 Fc-fusion proteins. Additionally, binding to a soluble target may not affect the PK of Fc-fusion proteins as the assays measured the total drug; also, a literature survey did not reveal the presence of high-level targets in the circulation. Third, compartmental analysis unified the nonlinear PK observed with IL-10 Fc-fusion proteins using the Michaelis-Menten kinetics that is commonly employed to describe TMDD. The *in vitro* binding affinity to the mIL-10 receptor alpha was used successfully as the Michaelis constant  $K_{m,target-mediated}$ , suggesting that nonlinear PK is related to the target. Fourth, the studies using a receptor-blocking antibody and a mutant with a reduced target binding affinity demonstrated a meaningful improvement in the terminal  $t_{1/2}$  of IL-10 Fc-fusion proteins, providing strong experimental evidence supporting the role of TMDD in the PK of these molecules. Finally, anti-drug antibodies for mFc-mIL-10 were detected  $\geq 7$  days upon repeat dosing (Supplemental Figure 5) and cannot explain rapid drug concentration declines within 2 days after dosing at low doses (0.03-0.05 mg/kg).

Compartmental modeling was applied to gain insight into the PK of IL-10 Fc-fusion proteins and IL-10. Dividing the target-mediated clearance ( $V_{max,target-mediated}/K_{m,target-mediated}$ ) by the  $V_c$  yielded a rate constant that reflects the target-mediated elimination. Using the values reported in Table 5, the target-mediated rate constant  $k_{target-mediated}$  was calculated to be 0.044 hours<sup>-1</sup> for mFc-mIL-10 and 0.081 hours<sup>-1</sup> for hFc-hIL-10. These values are ~2-fold apart, reflecting the comparable binding affinity values to the mIL-10 receptor alpha. When compared with the  $k_{non-target-mediated}$  (0.019-0.023 hours<sup>-1</sup>) of IL-10 Fc-fusion proteins, the  $k_{target-mediated}$  was 2.3- to 3.5- fold higher. These results suggest that when the IL-10 Fc-fusion protein concentrations are below the  $K_{m,target-mediated}$

mediated, target-mediated elimination plays a dominant role in governing the PK of these Fc-fusion proteins. In contrast, the  $k_{\text{non-target-mediated}}$  estimated for recombinant IL-10 proteins was 4.3-5.9 hours<sup>-1</sup> (Table 5). When these rate constants were compared with the  $k_{\text{target-mediated}}$  values mentioned above, the  $k_{\text{target-mediated}}$  was ~1% of the  $k_{\text{non-target-mediated}}$ . Naturally, the existence of TMDD cannot be detected in the IL-10 PK. Using the PK parameters of mFc-mIL-10 and mIL-10 presented in Table 5, the percentage of the TMDD contribution to the  $CL_{\text{tot}}$  in a range of concentrations was calculated and is shown in Figure 6. Between the concentrations of 1 and 10 nM, TMDD contributed to 36-64% of the  $CL_{\text{tot}}$  of mFc-mIL-10, whereas its contribution was <2% of the mIL-10  $CL_{\text{tot}}$  across the concentration range evaluated. The concentrations of 1 and 10 nM corresponded to the average concentration of mFc-mIL-10 over 2 to 3 weeks at the pharmacologically active dose of 0.1 and 0.3 mg/kg, respectively. At concentrations higher than 10 nM, the TMDD contribution to the mFc-mIL-10  $CL_{\text{tot}}$  diminished, indicating that TMDD is saturated. Although TMDD can be saturated at higher drug concentrations or doses, cautions need to be exercised on potential toxicity, because the therapeutic index is often narrow for cytokines (Berraondo et al., 2019).

In conclusion, TMDD played an important role in the PK of IL-10 Fc-fusion proteins at pharmacologically active doses. Compartmental modeling results and experimental evidence generated with a receptor-block antibody and a mutant strongly supported the conclusion. Future drug design with Fc-fusion proteins needs to consider target expression and examine its effect on PK. When conducting PK studies, a dose range covering pharmacological activity is crucial.

## **AUTHORSHIP CONTRIBUTIONS**

**Participated in research design:** Yang, Rajendran, Poirson, Gururajan, Loy, Vasudevan, Broz, Lehman-McKeeman, Morin, and Graziano

**Conducted experiments:** Rajendran, Spires, Poirson, Arbanas, Cheng, Carl, Pace, Wang, Mehl, and Xu

**Contributed new reagents or analytic tools:** Lin, Krystek, and Morin

**Performed data analysis:** Yang, Spires, Poirson, and Arbanas

**Wrote or contributed to the writing of the manuscript:** Yang, Rajendran, Spires, Poirson, Arbanas, Broz, Lehman-McKeeman, Morin, and Graziano

## REFERENCES

- Abdiche YN, Yeung YA, Chaparro-Riggers J, Barman I, Strop P, Chin SM, Pham A, Bolton G, McDonough D, Lindquist K, Pons J, Rajpal A (2015) The neonatal Fc receptor (FcRn) binds independently to both sites of the IgG homodimer with identical affinity. *MAbs* **7**:331-343.
- Alvarez HM, So OY, Hsieh S, Shinsky-Bjorde N, Ma H, Song Y, Pang Y, Marian M, Escandón E (2012) Effects of PEGylation and immune complex formation on the PK and biodistribution of recombinant interleukin 10 in mice. *Drug Metab Dispos* **40**:360-373.
- An G (2020) Concept of pharmacologic target-mediated drug disposition in large-molecule and small-molecule compounds. *J Clin Pharmacol* **60**:149-163.
- Adris S, Klein S, Jasniss M, Chuluyan E, Ledda M, Bravo A, Carbone C, Chernajovsky Y, Podhajcer O (1999) IL-10 expression by CT26 colon carcinoma cells inhibits their malignant phenotype and induces a T cell-mediated tumor rejection in the context of a systemic Th2 response. *Gene Ther* **6**:1705-1712.
- Berman RM, Suzuki T, Tahara H, Robbins PD, Narula SK, Lotze MT (1996) Systemic administration of cellular IL-10 induces an effective, specific, and long-lived immune response against established tumors in mice. *J Immunol* **157**:231-238.
- Berraondo P, Sanmamed MF, Ochoa MC, Etxeberria I, Aznar MA, Pérez-Gracia JL, Rodríguez-Ruiz ME, Ponz-Sarvisé M, Castañón E, Melero I (2019) Cytokines in clinical cancer immunotherapy. *Br J Cancer* **120**:6-15.
- Berzins SP, Boyd RL, Miller JF (1998) The role of the thymus and recent thymic migrants in the maintenance of the adult peripheral lymphocyte pool. *J Exp Med* **187**:1839-1848.
- Betts A, Keunecke A, van Steeg TJ, van der Graaf PH, Avery LB, Jones H, Berkhout J (2018) Linear pharmacokinetic parameters for monoclonal antibodies are similar within a species and across different pharmacological targets: a comparison between human, cynomolgus monkey and hFcRn Tg32 transgenic mouse using a population-modeling approach. *MAbs* **10**:751-764.
- Davies B and Morris T (1993) Physiological parameters in laboratory animals and humans. *Pharm Res* **10**:1093-1095.
- Emmerich J, Mumm JB, Chan IH, LaFace D, Truong H, McClanahan T, Gorman DM, Oft M (2012) IL-10 directly activates and expands tumor-resident CD8(+) T cells without de novo infiltration from secondary lymphoid organs. *Cancer Res* **72**:3570-3581.
- Hecht JR, Lonardi S, Bendell J, Sim HW, Macarulla T, Lopez CD, Van Cutsem E, Muñoz Martin AJ, Park JO, Greil R, Wang H, Hozak RR, Gueorguieva I, Lin Y, Rao S, Ryoo BY (2021) Randomized Phase III study of FOLFOX alone or with pegilodecakin as

- second-line therapy in patients with metastatic pancreatic cancer that progressed after gemcitabine (SEQUOIA). *J Clin Oncol* **39**:1108-1118.
- Huhn RD, Radwanski E, O'Connell SM, Sturgill MG, Clarke L, Cody RP, Affrime MB, Cutler DL (1996) PK and immunomodulatory properties of intravenously administered recombinant human interleukin-10 in healthy volunteers. *Blood* **87**:699-705.
- Intron<sup>®</sup> A package insert.
- Joyce AP, Wang M, Lawrence-Henderson R, Fillietaz C, Leung SS, Xu X, O'Hara DM (2014) One mouse, one pharmacokinetic profile: quantitative whole blood serial sampling for biotherapeutics. *Pharm Res* **31**:1823-1833.
- Jung K, Ha JH, Kim JE, Kim JA, Kim YJ, Kim CH, Kim YS (2018) Heterodimeric Fc-fused IL12 shows potent antitumor activity by generating memory CD8 + T cells. *Oncoimmunology* **7**:e1438800.
- Kontermann RE (2016) Half-life extended biotherapeutics. *Expert Opin Biol Ther* **16**:903-915.
- Kuna M, Mahdi F, Chade AR, Bidwell GL 3rd (2018) Molecular size modulates PK, biodistribution, and renal deposition of the drug delivery biopolymer elastin-like polypeptide. *Sci Rep* **8**:7923.
- Künze G, Köhling S, Vogel A, Rademann J, Huster D (2016) Identification of the glycosaminoglycan binding site of interleukin-10 by NMR spectroscopy. *J Biol Chem* **291**:3100-3113.
- Liu JY, Zhang XS, Ding Y, Peng RQ, Cheng X, Zhang NH, Xia JC, Zeng YX (2005) The changes of CD4+CD25+/CD4+ proportion in spleen of tumor-bearing BALB/c mice. *J Transl Med* **3**:5.
- Liu L (2018) PK of monoclonal antibodies and Fc-fusion proteins. *Protein Cell* **9**:15-32.
- Liu Y, Wei SH, Ho AS, de Waal Malefyt R, Moore KW (1994). Expression cloning and characterization of a human IL-10 receptor. *J Immunol* **152**:1821-1829.
- Moore KW, de Waal Malefyt R, Coffman RL, O'Garra A (2001) Interleukin-10 and the interleukin-10 receptor. *Annu Rev Immunol* **19**:683-765.
- Mumm JB, Emmerich J, Zhang X, Chan I, Wu L, Mauze S, Blaisdell S, Basham B, Dai J, Grein J, Sheppard C, Hong K, Cutler C, Turner S, LaFace D, Kleinschek M, Judo M, Ayanoglu G, Langowski J, Gu D, Paporello B, Murphy E, Sriram V, Naravula S, Desai B, Medicherla S, Seghezzi W, McClanahan T, Cannon-Carlson S, Beebe AM, Oft M (2011) IL-10 elicits IFN $\gamma$ -dependent tumor immune surveillance. *Cancer Cell* **20**:781-796.
- Naing A, Infante JR, Papadopoulos KP, Chan IH, Shen C, Ratti NP, Rojo B, Autio KA, Wong DJ, Patel MR, Ott PA, Falchook GS, Pant S, Hung A, Pekarek KL, Wu V, Adamow M, McCauley S, Mumm JB, Wong P, Van Vlasselaer P, Leveque J, Tannir NM, Oft M. (2018) PEGylated IL-10 (Pegilodecakin) Induces Systemic Immune Activation, CD8 + T

Cell Invigoration and Polyclonal T Cell Expansion in Cancer Patients. *Cancer Cell* **34**:775-791.

Proleukin® package insert.

Ray AL, Nofchissey RA, Khan MA, Reidy MA, Lerner MR, Wu X, Guo S, Hill SL, Weygant N, Adams SF, Castillo EF, Berry WL, Stout MB, Morris KT (2020). The role of sex in the innate and adaptive immune environment of metastatic colorectal cancer. *Br J Cancer* **123**:624-632.

Rhode PR, Egan JO, Xu W, Hong H, Webb GM, Chen X, Liu B, Zhu X, Wen J, You L, Kong L, Edwards AC, Han K, Shi S, Alter S, Sacha JB, Jeng EK, Cai W, Wong HC (2016) Comparison of the Superagonist Complex, ALT-803, to IL15 as Cancer Immunotherapeutics in Animal Models. *Cancer Immunol Res* **4**:49-60.

Roferon®-A package insert.

Runbeck E, Crescioli S, Karagiannis SN, Papa S (2021) Utilizing immunocytokines for cancer therapy. *Antibodies (Basel)* **10**:10.

Salek-Ardakani S, Arrand JR, Shaw D, Mackett M (2000) Heparin and heparan sulfate bind interleukin-10 and modulate its activity. *Blood* **96**:1879-1888.

Shouval DS, Ouahed J, Biswas A, Goettel JA, Horwitz BH, Klein C, Muise AM, Snapper SB (2014) Interleukin 10 receptor signaling: master regulator of intestinal mucosal homeostasis in mice and humans. *Adv Immunol* **122**:177-210.

Tan JC, Indelicato S, Narula SK, Zavodny PJ, Chou C-C (1993) Characterization of interleukin-10 receptors on human and mouse cells. *J Biol Chem* **268**:21053-21059.

Tannir NM, Papadopoulos KP, Wong DJ, Aljumaily R, Hung A, Afable M, Kim JS, Ferry D, Drakaki A, Bendell J, Naing A (2021) Pegilodecakin as monotherapy or in combination with anti-PD-1 or tyrosine kinase inhibitor in heavily pretreated patients with advanced renal cell carcinoma: Final results of cohorts A, G, H and I of IVY Phase I study. *Int J Cancer* **149**:403-408.

Unverdorben F, Richter F, Hutt M, Seifert O, Malinge P, Fischer N, Kontermann RE (2016) Pharmacokinetic properties of IgG and various Fc fusion proteins in mice. *MAbs* **8**:120-128.

Vazquez-Lombardi R, Loetsch C, Zinkl D, Jackson J, Schofield P, Deenick EK, King C, Phan TG, Webster KE, Sprent J, Christ D (2017) Potent antitumour activity of interleukin-2-Fc fusion proteins requires Fc-mediated depletion of regulatory T-cells. *Nat Commun* **8**:15373.

Vieira P and Rajewsky K (1988) The half-lives of serum immunoglobulins in adult mice. *Eur J Immunol* **18**:313-316.

- von Haehling S, Wolk K, Höflich C, Kunz S, Grünberg BH, Döcke WD, Reineke U, Asadullah K, Sterry W, Volk HD, Sabat R (2015) Interleukin-10 receptor-1 expression in monocyte-derived antigen-presenting cell populations: dendritic cells partially escape from IL-10's inhibitory mechanisms. *Genes Immun* **16**:8-14.
- Walter MR (2014) The molecular basis of IL-10 function: from receptor structure to the onset of signaling. *Curr Top Microbiol Immunol* **380**: 191-212.
- Wang F, Tsai JC, Davis JH, Chau B, Dong J, West SM, Hogan JM, Wheeler ML, Bee C, Morishige W, Cayton T, David-Brown D, Zhang C, Kozhich A, Sproul T, Dollinger G, Rajpal A, Strop P (2020) Design and characterization of mouse IgG1 and IgG2a bispecific antibodies for use in syngeneic models. *MAbs* **12**:1685350.
- Zhang Y, Huo M, Zhou J, Xie S (2010) PKSolver: An add-in program for pharmacokinetic and pharmacodynamic data analysis in Microsoft Excel. *Comput Methods Programs Biomed* **99**:306-314.
- Zhu EF, Gai SA, Opel CF, Kwan BH, Surana R, Mihm MC, Kauke MJ, Moynihan KD, Angelini A, Williams RT, Stephan MT, Kim JS, Yaffe MB, Irvine DJ, Weiner LM, Dranoff G, Wittrup KD (2015) Synergistic innate and adaptive immune response to combination immunotherapy with antitumor antigen antibodies and extended serum half-life IL-2. *Cancer Cell* **27**:489-501.

## FOOTNOTES

- a. The work was conducted as part of employment at Bristol Myers Squibb and no external funding was received.
- b. All authors are current or former employees of Bristol Myers Squibb and own or previously owned the company's stocks. The authors declare no conflict of interest with the contents of the article.



## FIGURE LEGENDS

Figure 1. Schematic structures of mFc-mIL-10 and hFc-hIL-10. Mutations were included in the Fc domains to eliminate or reduce antibody-dependent cellular cytotoxicity and complement-dependent cytotoxicity. For mFc-mIL-10, the Fc domain of murine immunoglobulin G1 (IgG1) had a single amino acid substitution of aspartic acid to alanine at codon 265 (D265A). For hFc-hIL-10, the Fc domain of human IgG1 (known as IgG1.3f) had 3 amino acid substitutions (L234A, L235E, and G237A). Both mouse IL-10 (mIL-10) and human IL-10 (hIL-10) were wild type and fused with the C-terminus of the Fc domain through a glycine-serine rich polypeptide linker to retain the activity of IL-10. The sequence structures and characterizations are available in Supplemental Data.

Figure 2. Plasma (or serum) concentration-time profiles of mFc-mIL-10 and hFc-hIL-10 in mice. a) intraperitoneal administration of mFc-mIL-10 at 0.03, 0.1, 0.3, 1, and 3-mg/kg doses to tumor-bearing mice in efficacy evaluations (N = 3-14 per time point, including data at 0.3 and 3 mg/kg obtained from non-tumor-bearing mice in the satellite groups of efficacy studies); b) intravenous dosing of mFc-mIL-10 at 0.05, 0.5, and 5-mg/kg doses to non-tumor-bearing mice (N = 4 per time point); and c) intravenous administration of hFc-hIL-10 at 0.05, 0.5, and 5-mg/kg doses to non-tumor-bearing mice (N = 4 per time point). Lines represent pharmacokinetic model-fitted average concentration-time curves. Symbols show individual observed data. When data points are less than the number of animals indicated or not shown in the figure, drug concentrations are below the LLOQ (0.08 nM for mFc-mIL-10 and 0.08 nM for hFc-hIL-10).

- Figure 3. Plasma concentration-time profiles of mIL-10 and hIL-10 in mice. a) intravenous dosing of mIL-10 at 0.05, 0.5, and 5-mg/kg doses to non-tumor-bearing mice (N = 4 per time point); b) intravenous administration of hIL-10 at 0.05, 0.5, and 5-mg/kg doses to non-tumor-bearing mice (N = 4 per time point). Lines represent pharmacokinetic model-fitted average concentration-time curves. Symbols show individual observed data. When data points are less than the number of animals indicated or not shown in the figure, drug concentrations are below the LLOQ (0.01 nM for mIL-10 and 0.1 nM for hIL-10).
- Figure 4. Target-mediated drug disposition of mFc-mIL-10 was blocked by an anti-mIL-10 receptor alpha antibody. a) Plasma concentration-time profiles of mFc-mIL-10 after intraperitoneal administration of a 0.1-mg/kg dose to mice in the presence and absence of an anti-mIL-10 receptor alpha antibody; b) Correlation between the AUC of mFc-mIL-10 and the doses of anti-mIL-10 receptor alpha antibody.
- Figure 5. Plasma concentration-time profiles of hFc-hIL-10 and an hFc-hIL-10 mutant after intraperitoneal administration of a 0.1-mg/kg dose to mice (N = 4 per time point). The line represents the average data in each group. Symbols show individual observed data. When data points are less than the number of animals indicated or not shown in the figure, drug concentrations are below the LLOQ (0.08 nM for hFc-hIL-10 and 0.5 nM for the hFc-hIL-10 mutant).
- Figure 6. Contribution of target-mediated drug disposition (TMDD) to the total clearance of mFc-mIL-10 and mIL-10. TMDD was assumed to be the same between the two molecules and the percentage of the TMDD contribution to the total clearance was calculated based on the parameters presented in Table 5. The dashed line

represents the average concentrations of mFc-mIL-10 over 2 to 3 weeks at its pharmacologically active dose of 0.1 mg/kg.

## TABLES

**Table 1. Molecular weight, binding affinity, and cellular activities of mFc-mIL-10 and hFc-hIL-10**

	mFc-mIL-10	hFc-hIL-10
MW (Dalton)	91,004	90,815
Binding affinity (nM) <sup>a</sup>		
Mouse IL-10 receptor alpha	3.2	2.9
Human IL-10 receptor alpha	No binding	0.6
Mouse neonatal Fc receptor	640 <sup>b</sup>	200
Human neonatal Fc receptor	No binding	1,100
In vitro cellular activity (nM)		
STAT3 phosphorylation in mouse CD3+ T cells	0.44	0.55
STAT3 phosphorylation in human CD3+ T cells	Not tested	0.24

a. Determined at 25°C and pH 7.2 for mouse and human IL-10 receptor alpha and 25°C and pH 6.0 for mouse and human neonatal Fc receptor.

b. Wang et al. (2019).

**Table 2. Pharmacokinetic parameters of mFc-mIL-10 after intraperitoneal administration to tumor-bearing mice in efficacy studies<sup>a</sup>**

	0.03 mg/kg (N = 4)	0.1 mg/kg (N = 14)	0.3 mg/kg <sup>b</sup> (N = 12)	1 mg/kg (N = 4)	3 mg/kg <sup>b</sup> (N = 3)
C <sub>max</sub> (nM)	0.9	10	41	170	500
C <sub>max</sub> ratio <sup>c</sup>	1.0	11	46	189	556
T <sub>max</sub> (h)	4	4	5	4	5
AUC <sub>tot</sub> (nM*d)	1.8	25	100	509	1686
AUC <sub>tot</sub> ratio <sup>c</sup>	1.0	14	56	283	937
Terminal t <sub>1/2</sub> (d)	1.0	1.2	1.5	2.2	2.7

a. Pharmacokinetic parameters were calculated based on the average concentration-time data from antitumor efficacy studies. Because a portion of the drug concentration data was obtained compositely, the standard deviation cannot be obtained for the pharmacokinetic parameters estimated.

b. Pharmacokinetic data from non-tumor-bearing mice in the satellite groups of an efficacy study were also included in the analysis (please see text for details).

c. The nominal dose ratio was 1:3.3:10:33:100; the non-specific adsorption-corrected dose ratio was 1:8.8:26:88:263 (see Table 5 for %drug remaining in dosing solution at 0.03 mg/kg estimated from compartmental modeling).

**Table 3. Pharmacokinetic parameters of mFc-mIL-10 and hFc-hIL-10 after intravenous administration to non-tumor-bearing mice**

	<b>mFc-mIL-10</b> <b>(mean ± SD, N = 4)</b>			<b>hFc-hIL-10</b> <b>(mean ± SD, N = 4)</b>		
	0.05 mg/kg <sup>a</sup>	0.5 mg/kg	5 mg/kg	0.05 mg/kg <sup>a</sup>	0.5 mg/kg	5 mg/kg
$C_{\max}$ (nM) <sup>b</sup>	3.0 ± 0.6	83 ± 23	789 ± 215	3.7 ± 0.5	77 ± 12	693 ± 168
C <sub>max</sub> ratio <sup>c</sup>	1.0	28	263	1.0	21	187
AUC <sub>tot</sub> (nM*d)	0.9 ± 0.3	164 ± 50	1651 ± 136	1.8 ± 0.1	135 ± 16	1,139 ± 221
AUC <sub>tot</sub> ratio <sup>c</sup>	1.0	181	1830	1.0	75	633
CL <sub>tot</sub> (mL/d/kg)	239 ± 65	36 ± 10	33 ± 2.6	162 ± 8.5	41 ± 4.8	50 ± 10
V <sub>ss</sub> (mL/kg)	78 ± 19	124 ± 32	178 ± 28	106 ± 5.2	161 ± 50	141 ± 25
Terminal t <sub>1/2</sub> (d)	0.22 ± 0.018	2.6 ± 0.55	3.9 ± 0.47	0.45 ± 0.039	2.9 ± 1.1	2.0 ± 0.83

- a. The dose of 0.05 mg/kg was corrected for drug loss due to nonspecific adsorption in dosing vials and devices. The actual dose used for PK parameter estimations was 0.019 mg/kg for mFc-mIL-10 and 0.026 mg/kg for hFc-hIL-10. These doses were estimated using compartmental modeling (Table 5 and please see text for additional details).
- b. First sampling time point (3 min) after an IV bolus dose.
- c. The nominal dose ratio was 1:10:100; the nonspecific adsorption-corrected dose ratio for mFc-mIL-10 and hFc-hIL-10 was 1:26:263 and 1:19:192, respectively.

**Table 4. Pharmacokinetic parameters of mIL-10 and hIL-10 after intravenous administration to non-tumor-bearing mice**

	<b>mIL-10</b> <b>(mean ± SD, N = 4)</b>			<b>hIL-10</b> <b>(mean ± SD, N = 3-4)</b>		
	0.05 mg/kg <sup>a</sup>	0.5 mg/kg	5 mg/kg	0.05 mg/kg <sup>a</sup>	0.5 mg/kg	5 mg/kg
$C_{\max}$ (nM) <sup>b</sup>	5.3 ± 1.0	218 ± 91	2,161 ± 397	7.0 ± 0.81	141 ± 33	1,513 ± 380
$C_{\max}$ ratio <sup>c</sup>	1.0	41	408	1.0	20	216
AUC <sub>tot</sub> (nM*d)	0.089 ± 0.011	3.7 ± 2.0	34 ± 7.9	0.067 ± 0.002	1.5 ± 0.27	18 ± 2.8
AUC <sub>tot</sub> ratio <sup>c</sup>	1.0	42	382	1.0	22	269
CL <sub>tot</sub> (mL/d/kg)	3,836 ± 480	4,341 ± 1732	4,085 ± 941	8,640 ± 208	8,925 ± 1,485	7,557 ± 1,188
V <sub>ss</sub> (mL/kg)	103 ± 54	139 ± 45	143 ± 38	77 ± 13	193 ± 68	209 ± 112
Terminal t <sub>1/2</sub> (d)	0.034 ± 0.031 <sup>d</sup>	0.067 ± 0.006	0.066 ± 0.016	0.008 ± 0.001 <sup>c</sup>	0.045 ± 0.019	0.049 ± 0.010

a. The dose of 0.05 mg/kg was corrected for drug loss due to nonspecific adsorption in dosing vials and devices. The actual dose used for PK parameter estimations was 0.013 mg/kg for mIL-10 and 0.022 mg/kg for hIL-10. These doses were estimated using compartmental modeling (Table 5 and please see text for additional details).

b. First sampling time point (3 min) after an IV bolus dose.

c. The nominal dose ratio was 1:10:100; the nonspecific adsorption-corrected dose ratio for mIL-10 and hIL-10 was 1:40:400 and 1:23:227, respectively.

d. Due to the assay sensitivity, the terminal t<sub>1/2</sub> estimated at the 0.05-mg/kg dose may not represent the terminal phase.

**Table 5. Compartmental analysis of mFc-mIL-10, mIL-10, hFc-hIL-10, and hIL-10 pharmacokinetic data in tumor- and non-tumor-bearing mice**

	<b>mFc-mIL-10</b> (mean ± SD)	<b>mIL-10</b> (mean ± SD)	<b>hFc-hIL-10</b> (mean ± SD)	<b>hIL-10</b> (mean ± SD)
<b>IV</b>				
$V_c$ (mL/kg)	69 ± 3.5	35 ± 0.23	81 ± 1.9	58 ± 0.65
$k_{12}$ (1/h)	0.213 ± 0.041	1.6 ± 0.034	0.13 ± 0.017	2.6 ± 0.12
$k_{21}$ (1/h)	0.209 ± 0.048	0.88 ± 0.019	0.16 ± 0.023	1.2 ± 0.038
$k_{el, \text{ non-target-mediated}}$ (1/h)	0.019 ± 0.0022	4.3 ± 0.030	0.023 ± 0.00091	5.9 ± 0.097
$K_{m, \text{ target-mediated}}$ (nM)	3.2 (fixed) <sup>b</sup>	Not applicable	2.9 (fixed) <sup>b</sup>	Not applicable
$V_{\text{max, target-mediated}}$ (nmol/kg/h)	0.0098 ± 0.0013	Not applicable	0.019 ± 0.0030	Not applicable
%drug remaining in dosing solution at 0.05 mg/kg <sup>a</sup>	38 ± 1.8	25 ± 1.6	52 ± 2.8	44 ± 2.7
<b>IP</b>				
$k_a$ (1/h)	0.25 ± 0.039	Not applicable	Not applicable	Not applicable
$V_{c, \text{ apparent}}$ (mL/kg) <sup>c</sup>	45 ± 3.0	Not applicable	Not applicable	Not applicable
%drug remaining in dosing solution at 0.03 mg/kg <sup>a</sup>	38 ± 1.8	Not applicable	Not applicable	Not applicable

a. The drug loss due to non-specific drug adsorption to dosing vials and devices at the low doses of 0.03 - 0.05 mg/kg was estimated from fitting the data. The estimations were supported by the in vitro results where the %drug remaining in a dosing solution of 0.02 mg/mL (0.1 mg/kg with a dosing volume of 5 mL/kg) after 2 hours at room temperature was found to be 60%.

b. In vitro IL-10 receptor alpha binding affinity  $K_d$  determined by a surface plasmon resonance method.

c.  $V_{c, \text{ apparent}}$ , as opposed to the IP bioavailability, was used as a parameter to model the data after IP administration. As described in the text, the IP bioavailability after the simultaneous fitting of the mFc-mIL-10 IV and IP data was estimated



to be >100% across a wide dose range (0.03 - 3 mg/kg), indicating a systematic difference between the IV and IP studies. Therefore, the  $V_{c,apparent}$  was used as a scalar and a more appropriate parameter to fit the IP data.

Table 6. Pharmacokinetic parameters of hFc-hIL-10 and a mutant of hFc-hIL-10 after intraperitoneal administration of 0.1 mg/kg to non-tumor-bearing mice

	hFc-hIL-10 (mean $\pm$ SD, N = 4)	hFc-hIL-10 mutant (mean $\pm$ SD, N = 4)
Binding affinity (nM) to human IL-10 receptor alpha	0.6	2,300
C <sub>max</sub> (nM)	16 $\pm$ 2.8	61 $\pm$ 10
T <sub>max</sub> (h)	9.0 $\pm$ 10	4.0 $\pm$ 0.0
AUC <sub>tot</sub> (nM*d)	32 $\pm$ 7.9 <sup>a</sup>	200 $\pm$ 54
Terminal t <sub>1/2</sub> (d)	0.71 $\pm$ 0.10 <sup>a</sup>	1.9 $\pm$ 0.57

a. The AUC<sub>tot</sub> and terminal t<sub>1/2</sub> shown were approximated values due to an accelerated drug concentration drop at the last measurable time point for hFc-hIL-10.

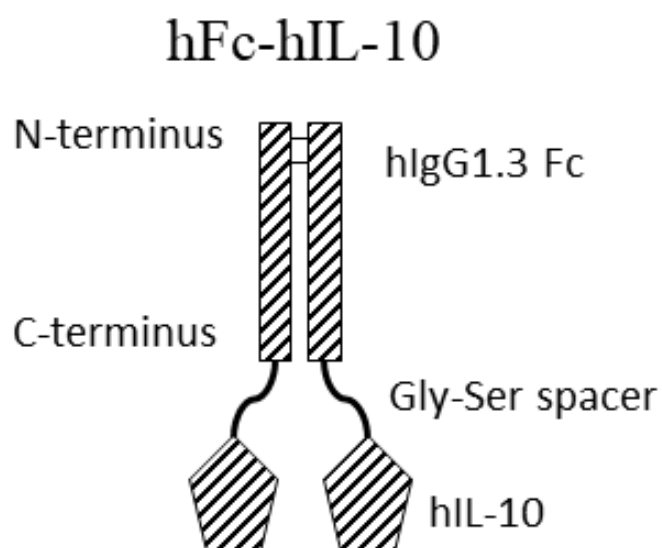
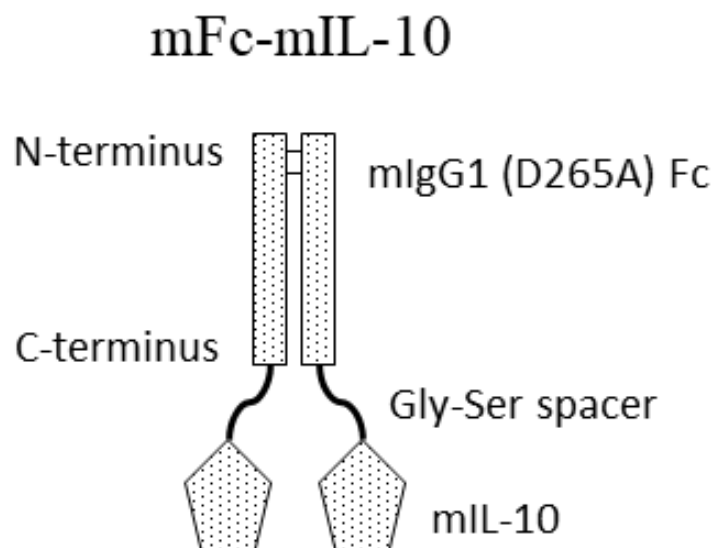


Figure 1

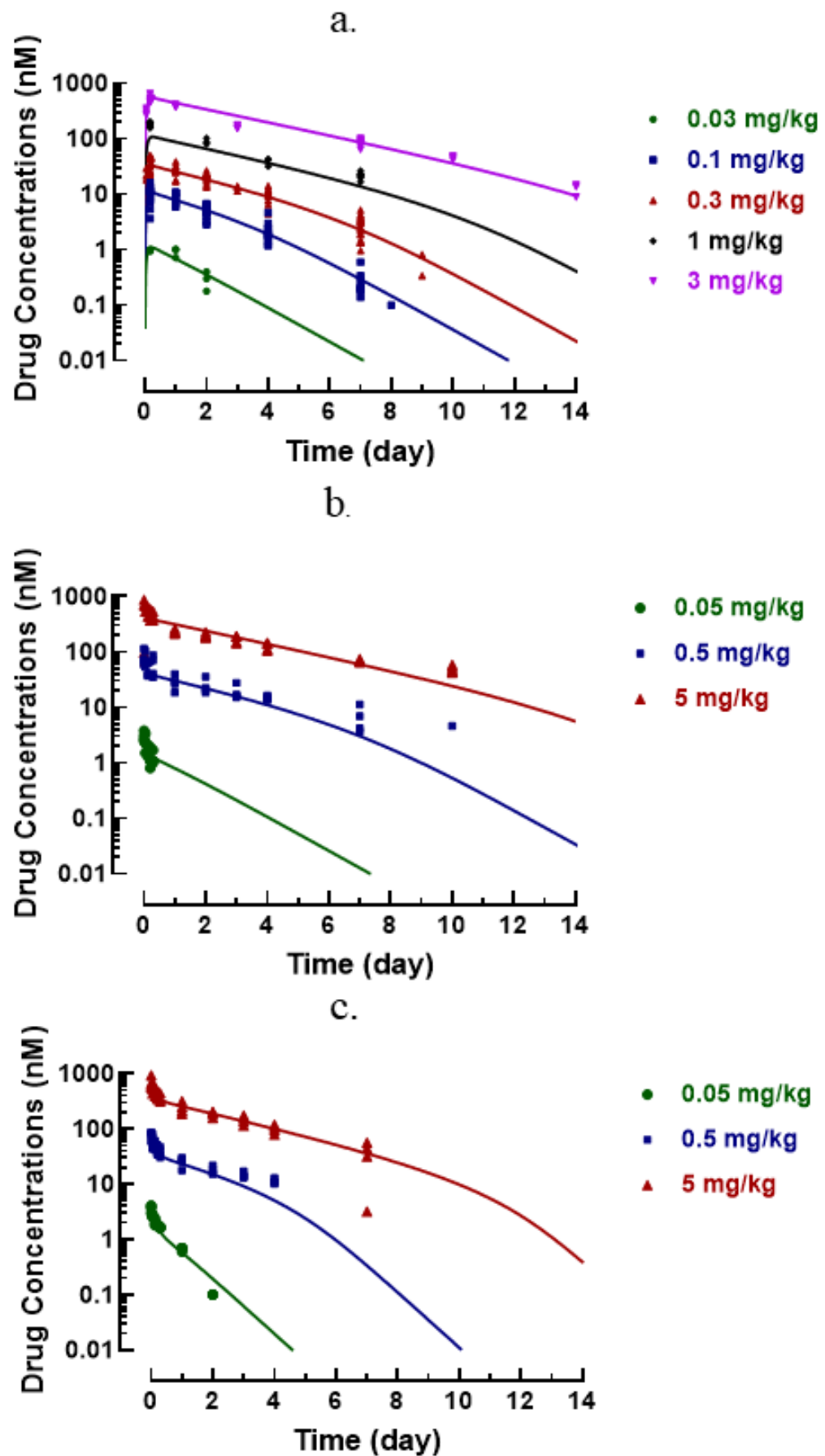


Figure 2

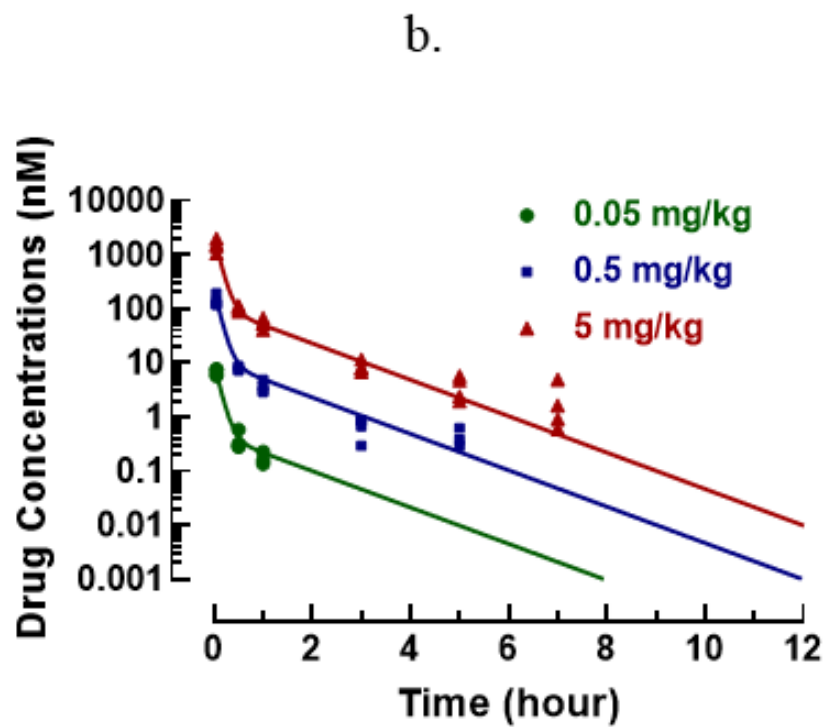
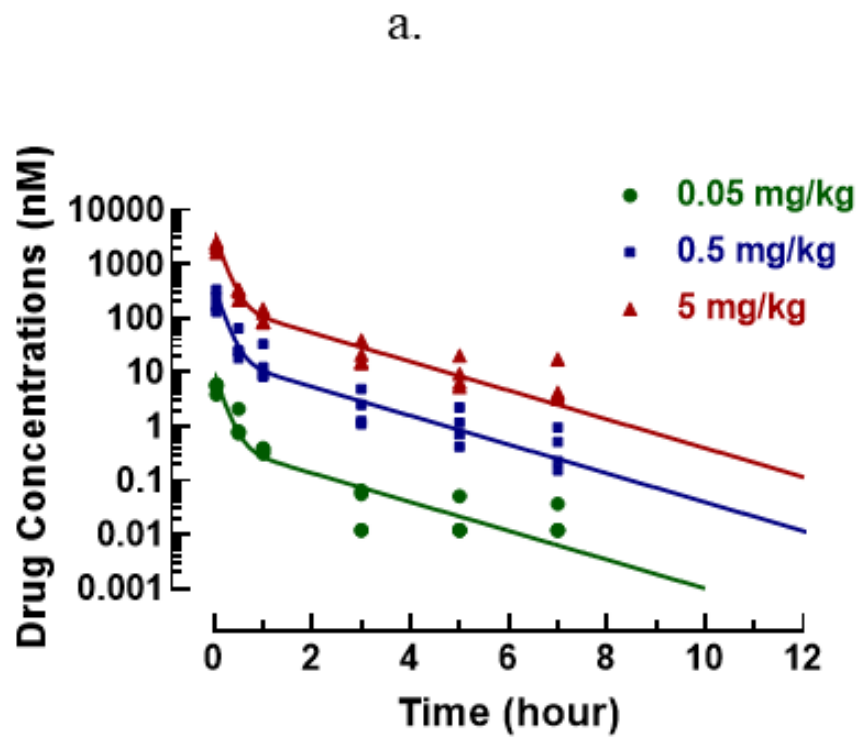
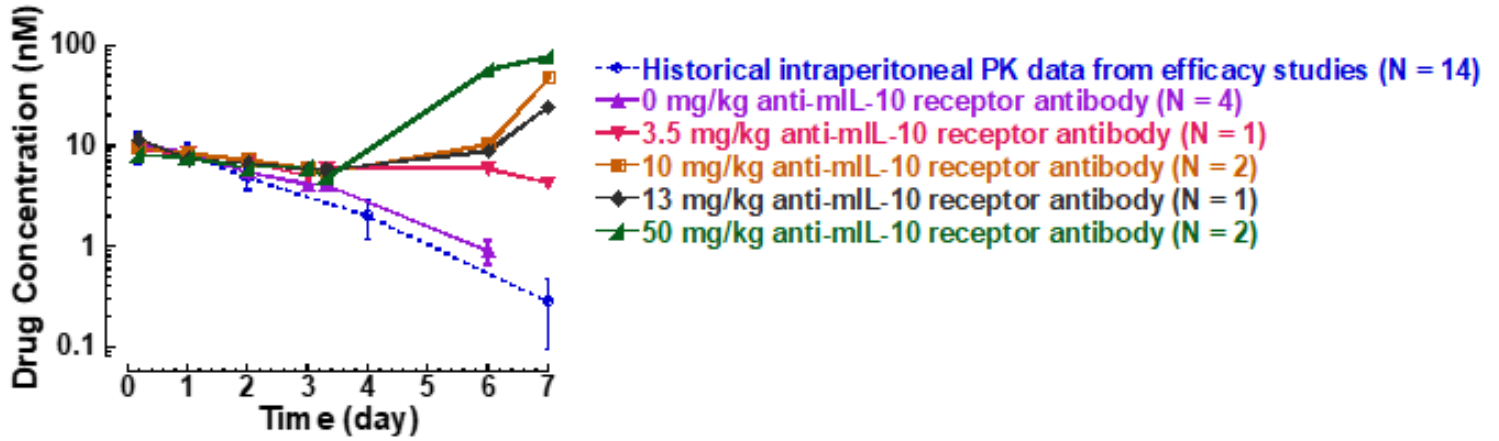


Figure 3

a.



b.

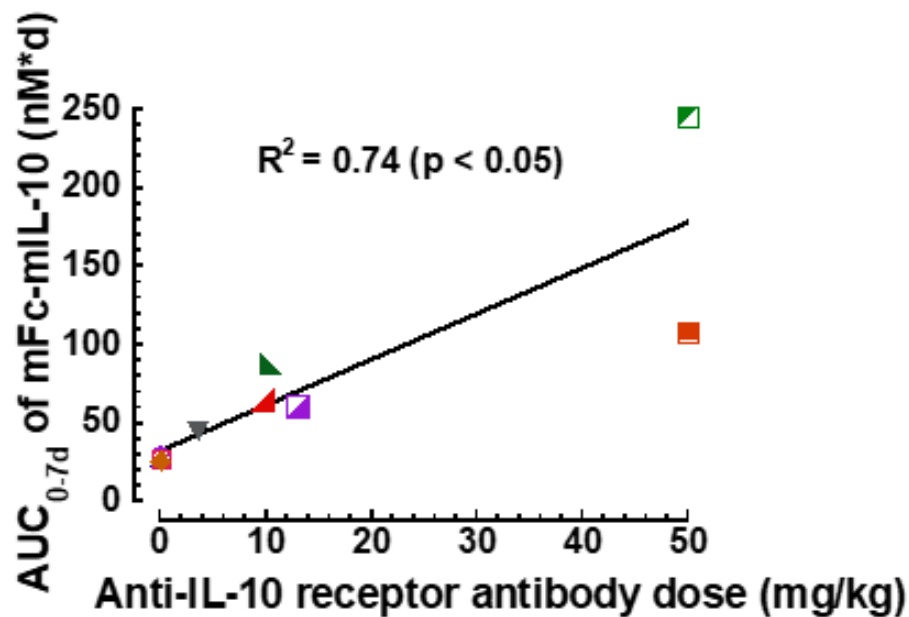


Figure 4

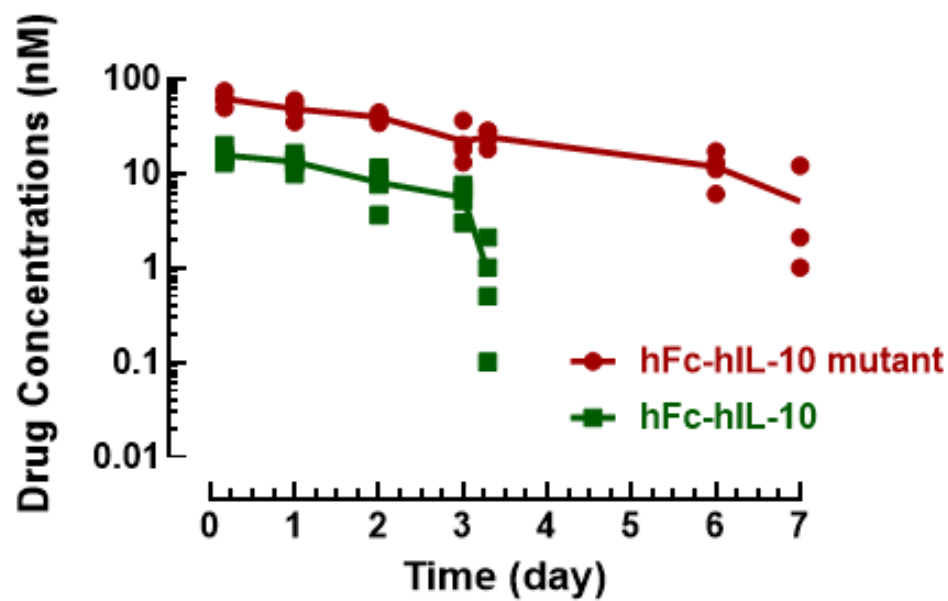


Figure 5

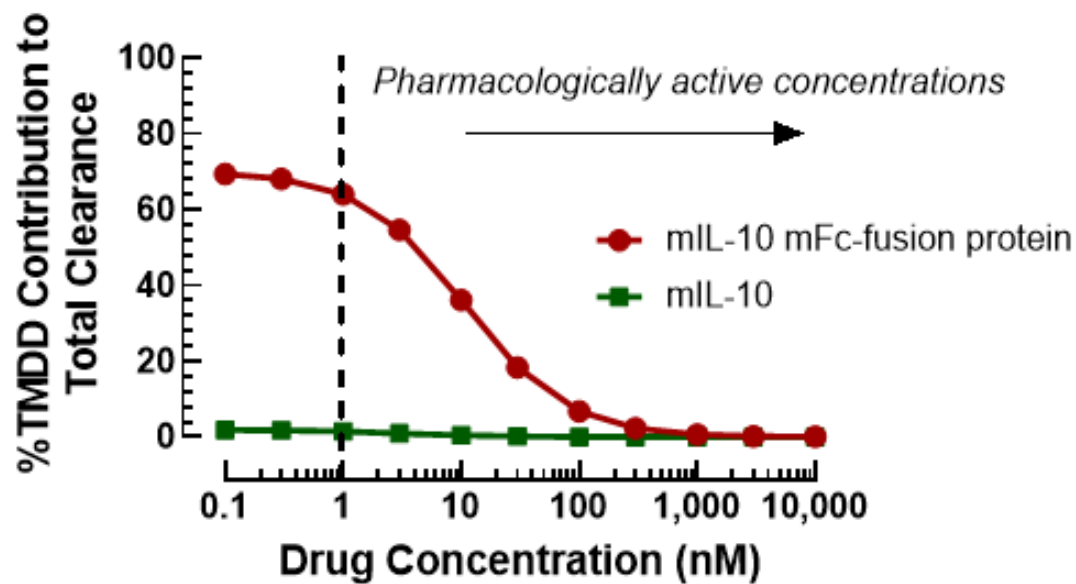


Figure 6



**Target-Mediated Drug Disposition Affects the Pharmacokinetics of Interleukin-10**

**Fc-fusion Proteins at Pharmacologically Active Doses**

**Authors:** Zheng Yang, Surendran Rajendran, Vanessa Spires, Brian Poirson, Murali Gururajan, Zheng Lin, Jaren Arbanas, Stanley Krystek, James Loy, Yuan Cheng, Stephen Carl, Samantha Pace, Yun Wang, John Mehl, Shihua Xu, Krishna Vasudevan, Miranda Broz, Lois Lehman-McKeeman, Paul Morin, and Robert F. Graziano

**Affiliation:** Bristol Myers Squibb Company, Princeton, New Jersey, U.S.A.

**SUPPLEMENTAL MATERIALS AND REAGENTS**

**1. Structural Sequences of IL-10 and IL-10 Fc-fusion Proteins**

**mIL-10**

```
1      SRGQY SREDN NCTHF PVGQS HMLLE LRTAF SQVKT FFQTK
41     DQLDN ILLTD SLMQD FKGYL GCQAL SEMIQ FYLVE VMPQA
81     EKHGP EIKEH LNSLG EKLKT LRMRL RRCHR FLPCE NKSKA
121    VEQVK SDFNK LQDQG VYKAM NEFDI FINCI EAYMM IKMKS
```

**hIL-10**

```
1      SRGQG TQSEN SCTHF PGNLP NMLRD LRDAF SRVKT FFQMK
41     DQLDN LLLKE SLLED FKGYL GCQAL SEMIQ FYLEE VMPQA
81     ENQDP DIKAH VNSLG ENLKT LRLRL RRCHR FLPCE NKSKA
121    VEQVK NAFNK LQEKG IYKAM SEFDI FINYI EAYMT MKIRN
```

**mFc-mIL-10**

```
1      VPRDCGCKPC ICTVPEVSSV FIFPPKPKDV LTITLTPKVT CVVVAISKDD
51     PEVQFSWFVD DVEVHTAQTQ PREEQFNSTF RSVSELPIMH QDWLNGKEFK
101    CRVNSAAFPA PIEKTISKTK GRPKAPQVYT IPPPKQMAK DKVSLTCMIT
151    DFFPEDITVE WQWNGQPAEN YKNTQPIMDT DGSYFVYSKL NVQKSNWEAG
201    NTFTCSVLHE GLHNHHTES LSHSPGGGGG SGGGSGGGG SGGGSSRGQ
251    YSREDNNCTH FPGVQSHMLL ELRTAFSQVK TFFQTKDQLD NILLTDSLMO
301    DFKGYLGCA LSEMIQFYL EVMPQAEKHG PEIKEHLNSL GEKLKTLRMR
351    LRRCHRFLPC ENKSKAVEQV KSDFNKLQDQ GVKAMNEFD IFINCIEAYM
401    MIKMKS
```

### hFc-hIL-10

```
1      DKTHTCPPCP APEAEGAPSV FLFPPKPKDT LMISRTPEVT CVVVDVSHED
51     PEVKFNWYVD GVEVHNAKTK PREEQYNSTY RVVSVLTVLH QDWLNGKEYK
101    CKVSNKALPA PIEKTISKAK GQPREPQVYT LPPSREEMTK NQVSLTCLVK
151    GFYPSDIAVE WESNGQPENN YKTTTPVLDS DGSFFLYSKL TVDKSRWQQG
201    NVFSCSVMHE ALHNHYTQKS LSLSPGGGGG SSGGGGSGGG GSGGGGSSPG
251    QGTQSENSCT HFPGNLPNML RDLRDAFSRV KTFFQMKDQL DNLLKESLL
301    EDFKGYLGCQ ALSEMIQFYL EEVMPQAENQ DPDIKAHVNS LGENLKTLLR
351    RLRRCHRFLP CENKSKAVEQ VKNAFNKLQE KGIYKAMSEF DIFINYIEAY
401    MTMKIRN
```

### hFc-hIL-10 mutant

```
1      DKTHTCPPCP APEAEGAPSV FLFPPKPKDT LMISRTPEVT CVVVDVSHED
51     PEVKFNWYVD GVEVHNAKTK PREEQYNSTY RVVSVLTVLH QDWLNGKEYK
101    CKVSNKALPA PIEKTISKAK GQPREPQVYT LPPSREEMTK NQVSLTCLVK
151    GFYPSDIAVE WESNGQPENN YKTTTPVLDS DGSFFLYSKL TVDKSRWQQG
201    NVFSCSVMHE ALHNHYTQKS LSLSPGGGGG SSGGGGSGGG GSGGGGSSPG
251    QGTQSENSCT HFPGNLPNML SDLRDAFSRV KTFFSMKDQL DNSLLKESLL
301    EDFKGYLGCQ ALSEMIQFYL EEVMPQAENQ DPDIKAHVNS LGENLKTLLR
351    RLRRCHRFLP CENKSKAVEQ VKNAFNKLQE KGIYKAMSEF DIFINYIEAY
401    MTMKIRN
```

## 2. Characterizations of IL-10 and IL-10 Fc-fusion Proteins

	mIL-10	hIL-10	mFc-mIL-10	hFc-hIL-10	hFc-hIL-10 Mutant
<b>Molecular Weight (Da)*</b>	18,751	18,703	91,004	90,815	90,542
<b>Aggregation status</b>					
<b>High molecular weight aggregates</b>	<5%	<5%	<5%	<5%	<5%
<b>Low molecular weight components</b>	<5%	<5%	<5%	<5%	<5%
<b>Endotoxin (EU/mL)</b>	<0.075	<0.075	<0.075	<0.075	<0.075

\*Theoretical mass of deglycosylated form.

Primary structures of all five protein analytes (mIL-10, hIL-10, mFc-mIL-10, hFc-hIL10, and hFc-hIL-10 mutant) used in this publication were confirmed by LC/MS/MS peptide mapping with >97% sequence coverage. The molecular weights of the intact versions of these proteins verified by LC/MS were consistent with the theoretical masses calculated from the respective protein amino acid sequences.

## SUPPLEMENTAL TABLE

**Supplemental Table 1. Key Models Tested and Fitting Performance for mFc-mIL-10 Pharmacokinetic Data after Intravenous and Intraperitoneal Administration to Tumor- and Non-tumor-bearing Mice**

Model	Objective function <sup>a,b</sup>	Akaike information criterion <sup>b</sup>	Schwarz-Bayesian information criterion <sup>b</sup>
1-compartment model with target- and non-target-mediated elimination	839	869	897
2-compartment model with target-mediated elimination only	839	870	900
2-compartment model with target- and non-target-mediated elimination ( <b>final model</b> )	812	842	874

a. Expressed as -2 times the log-likelihood function.

b. Converted from the output statistics in SAAM II.

**Supplemental Table 2. Key Models Tested and Fitting Performance for hFc-hIL-10 Pharmacokinetic Data after Intravenous Administration to Non-tumor-bearing Mice**

Model	Objective function <sup>a,b</sup>	Akaike information criterion <sup>b</sup>	Schwarz-Bayesian information criterion <sup>b</sup>
1-compartment model with target- and non-target-mediated elimination	409	424	432
2-compartment model with target-mediated elimination only	407	422	432
2-compartment model with target- and non-target-mediated elimination ( <b>final model</b> )	357	375	387

a. Expressed as -2 times the log-likelihood function.

b. Converted from the output statistics in SAAM II.

**Supplemental Table 3. Key Models Tested and Fitting Performance for mIL-10 Pharmacokinetic Data after Intravenous Administration to Non-tumor-bearing Mice**

Model	Objective function <sup>a,b</sup>	Akaike information criterion <sup>b</sup>	Schwarz-Bayesian information criterion <sup>b</sup>
1-compartment model with non-target-mediated elimination only	4,335	4,320	4,320
2-compartment model with target- and non-target-mediated elimination <sup>c</sup>	404	414	421
2-compartment model with non-target-mediated elimination only ( <b>final model</b> )	407	418	421

a. Expressed as -2 times the log-likelihood function.

b. Converted from the output statistics in SAAM II.

c. The target binding affinity of mIL-10 was assumed to be the same as that (3.2 nM) of mFc-mIL-10 in mice.

**Supplemental Table 4. Key Models Tested and Fitting Performance for hIL-10 Pharmacokinetic Data after Intravenous Administration to Non-tumor-bearing Mice**

<b>Model</b>	<b>Objective function<sup>a,b</sup></b>	<b>Akaike information criterion<sup>b</sup></b>	<b>Schwarz-Bayesian information criterion<sup>b</sup></b>
1-compartment model with non-target-mediated elimination only	2,490	2,492	2,492
2-compartment model with target- and non-target-mediated elimination <sup>c</sup>	261	273	277
2-compartment model with non-target-mediated elimination only ( <b>final model</b> )	280	290	294

a. Expressed as -2 times the log-likelihood function.

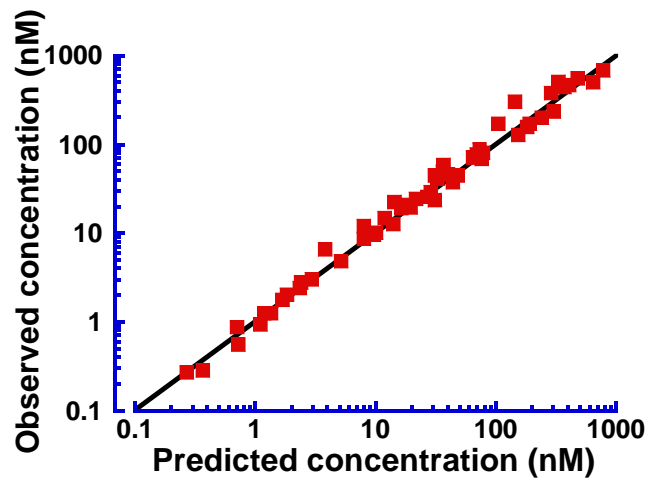
b. Converted from the output statistics in SAAM II.

c. The target binding affinity of hIL-10 was assumed to be the same as that (2.9 nM) of hFc-hIL-10 in mice.

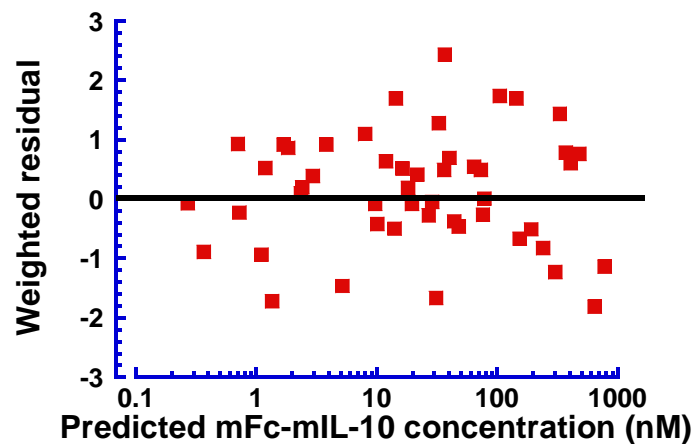
## SUPPLEMENTAL FIGURE

**Supplemental Figure 1. Diagnostic Plots Obtained from Pharmacokinetic Modeling of mFc-mIL-10 Average Concentration Data after Intravenous and Intraperitoneal Administration to Tumor- and Non-tumor-bearing Mice**

a. Predicted vs. observed concentrations

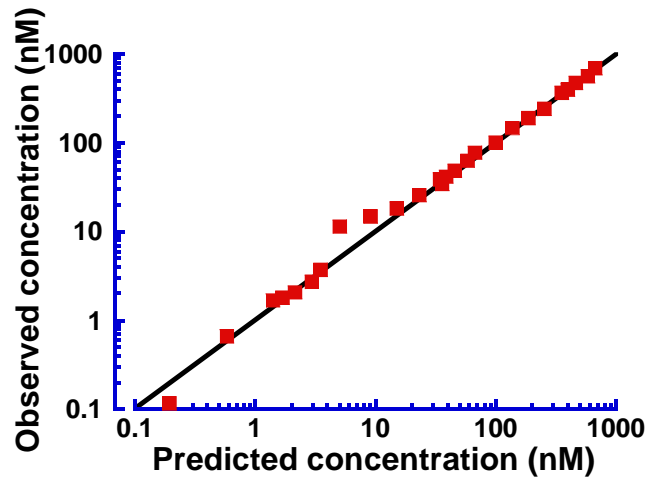


b. Weighted residuals vs. predicted concentrations

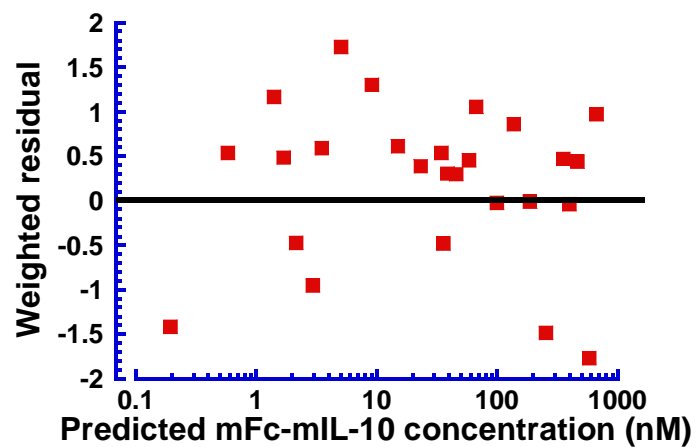


**Supplemental Figure 2. Diagnostic Plots Obtained from Pharmacokinetic Modeling of hFc-hIL-10 Average Concentration Data after Intravenous Administration to Non-tumor-bearing Mice**

a. Predicted vs. observed concentrations

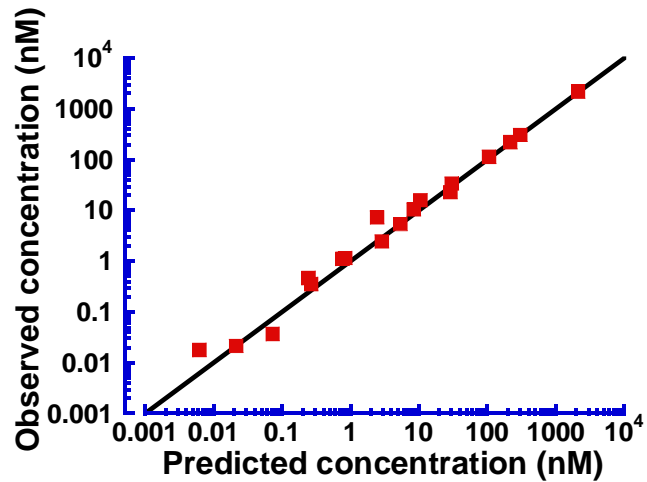


b. Weighted residuals vs. predicted concentrations

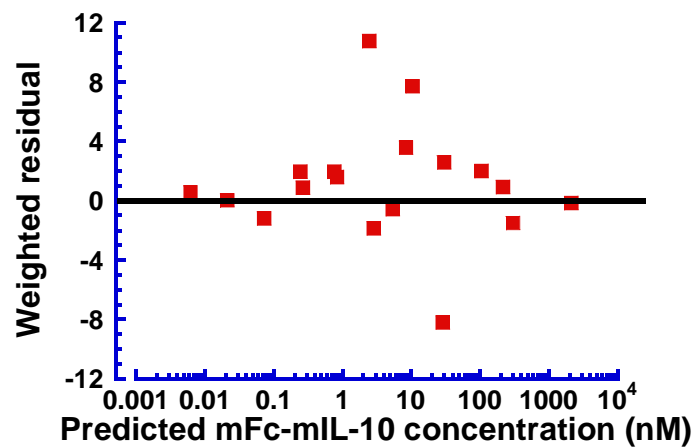


**Supplemental Figure 3. Diagnostic Plots Obtained from Pharmacokinetic Modeling of mIL-10 Average Concentration Data after Intravenous Administration to Non-tumor-bearing Mice**

a. Predicted vs. observed concentrations

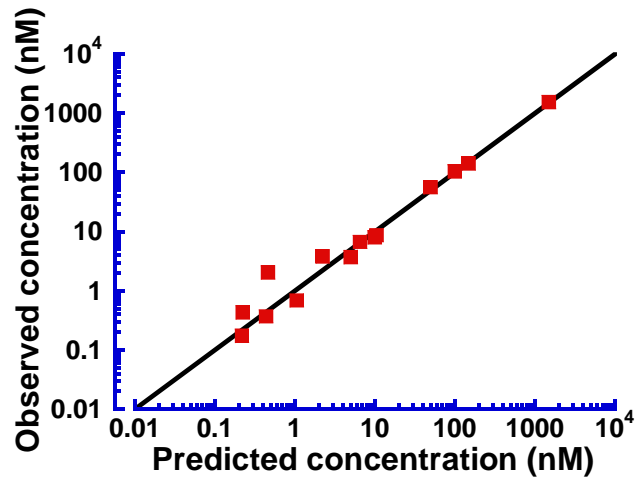


b. Weighted residuals vs. predicted concentrations

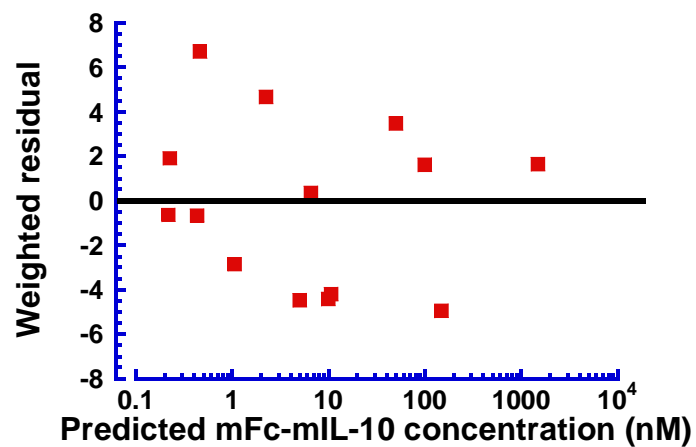


**Supplemental Figure 4. Diagnostic Plots Obtained from Pharmacokinetic Modeling of hIL-10 Average Concentration Data after Intravenous Administration to Non-tumor-bearing Mice**

a. Predicted vs. observed concentrations



b. Weighted residuals vs. predicted concentrations





**Supplemental Figure 5. Time Course of Anti-mFc-mIL-10 Antibody Titers in the Mouse CT26 Syngeneic Tumor Model following Intraperitoneal Administration of mFc-mIL-10 and a Mouse Anti-mPD-1 Monoclonal Antibody**

(Note: mFc-mIL-10 was dosed weekly (QW) for 3 doses and the mouse anti-mPD-1 monoclonal antibody was given every 4 days (Q4D) for 6 doses. Anti-mFc-mIL-10 antibodies in mouse serum samples were detected by a ligand-binding assay on a chemiluminescence platform developed at Bristol Myers Squibb, with mFc-mIL-10 and peroxidase AffiniPure rat anti-mouse IgG (H+L) (Jackson ImmunoResearch Laboratories Inc., West Grove, PA) used as the capture and detection reagents, respectively. The line represents the average value of the data.)

